The Dissertation Committee for Ming Xie
certifies that this is the approved version of the following dissertation:

Direct Electrical Control of Exciton and Polariton Condensates

Committee:

Allan H. MacDonald, Supervisor

Alexander A. Demkov

Gregory A. Fiete

Emanuel Tutuc

Jianshi Zhou

Direct Electrical Control of Exciton and Polariton Condensates

by

Ming Xie

DISSERTATION

Presented to the Faculty of the Graduate School of

The University of Texas at Austin

in Partial Fulfillment

of the Requirements

for the Degree of

DOCTOR OF PHILOSOPHY

THE UNIVERSITY OF TEXAS AT AUSTIN

August 2017

To my parents and sister

Acknowledgments

I am deeply grateful to many people who have supported me and walked along with me on this adventurous road. Without them I would not make it to see this milestone.

First and foremost, I would like to thank my advisor Allan MacDonald. He is a great mentor and has always been a great inspiration to me through these years of training and exploration. His immense knowledge has provided me a high-reaching ladder to see a much broader and more profound world of physics. I'm truly glad that I had this chance to come to Austin and complete my graduate study under Allan's guidance.

I also want to express my sincere gratitude to our experimental collaborators, David Snoke and Emanuel Tutuc. I appreciate those many discussions we had from which I learned important lessons on how to communicate and cooperate with experimental colleagues.

I am very thankful to have many wonderful colleagues from the theory group. I want to first express my special thanks to Guru Khalsa who has helped me greatly at the beginning of my PhD study. I very much enjoyed working with him. I also want to thank Xiao Li from whom I had learned a lot outside my research area. I enjoyed valuable times and interactions with my current and former colleagues: Yasufumi Araki, Hua Chen, Ran

Cheng, Gaurav Chaudhary, Dmitry Efimkin, Rohit Hedge, Pantelis Lapas, Chao Lei, Timothy Lovorn, Massoud Masir, Akihiko Sekine, Ashley da Silva, Inti Sodemann, Jung-jung Su, John Tolsma, Jun Wen, Fengcheng Wu, Fei Xue and Jihang Zhu.

I would also like to thank people who have served on my dissertation committee: Alex Demkov, Greg Fiete, Qian Niu, Emanuel Tutuc and Jianshi Zhou for their kind and generous support especially during these final days of my graduate study.

My gratitude also goes to our current and former staff members Becky Drake, Michele Landfield and Jane Ann Parker. Michele has created for us a nice and comfortable office environment to work in and made all the non-research works much easier and smoother.

Finally, to my dear parents and sister, words are never enough.

Direct Electrical Control of Exciton and Polariton Condensates

Publication No. _____

Ming Xie, Ph.D.
The University of Texas at Austin, 2017

Supervisor: Allan H. MacDonald

Excitons are among the most ubiquitous bosonic quasiparticle excitations in solid state systems whose lifetime can be extended such that quasi-thermal equilibrium states can be reached. They have thus been promising subjects for the study of Bose-Einstein condensation (BEC) physics during the last few decades. Indeed, convincing evidence for BEC of excitons and exciton polaritons, which are coupled state of quantum-well excitons and cavity photons, have been reported. In this dissertation, we study the property of two dimensional exciton and exciton-polariton condensates driven by external electric bias and discuss possible electro-optic device applications.

In the first chapter, we give a brief introduction to the basic concept of excitons, exciton-polaritons and their condensation, each followed by a short survey of the past and ongoing researches in their respective fields.

The second chapter presents our study on the electrically controlled coherent excitonic steady state in two dimensional transition-metal dichalco-

genide (TMD) double-layer system. We point out that a pair of electrical contacts with chemical potentials separated by less than the spatially indirect band gap of a 2D double-layer can be used to establish an exciton reservoir with an electrically controlled chemical potential. Equilibration between the exciton fluid and the contacts proceeds via a process involving virtual intermediate states in which an unpaired electron or hole occupies a free carrier state in one of the 2D layers. We relate the equilibration rate between excitons and contacts to the tunneling conductances between the contacts and the individual 2D layers when the contact chemical potentials align with the free-carrier bands. As an initial exploration of how spatially indirect 2D exciton systems can be studied and manipulated electrically, we explain how *dc* and *ac* voltage variation can be used to measure thermodynamic properties of the exciton fluid and to characterize the strength of its coupling to the reservoir.

In the third chapter, we study the thermo-electric transport properties of excitons. Based on the two-particle tunneling process discussed in previous chapter, we propose a possible realization of a thermo-electric cooling device in which indirect excitons act as the heat carriers. Excitons are injected from the cold side of the device and flow downhill a chemical potential gradient, which is maintained by the bias voltage difference set up between the cold and the hot side, to the hot side where they break into individual electrons and holes exiting to the electrodes.

In the fourth chapter, we present a theory of exciton or exciton-polariton supercurrent generation. We describe a mechanism by which an electrical bias

voltage applied across a unipolar semiconductor quantum well can drive an exciton or polariton supercurrent. The mechanism depends on the properties of electronic quasiparticles in quantum wells or two-dimensional materials when they are dressed by interactions with the coherent exciton field of an exciton condensate or the coherent exciton and photon fields of a polariton condensate, and on approximate conservation of the sum of the total photon and exciton numbers. We propose experiments that can be performed to realize this new light-matter coupling effect, and discuss possible applications. Assuming the dominant process for electron transfer between conduction and valence bands is by scattering off the condensate, electrical bias voltages can be used to control the condensate. We study the in-plane transport properties of electrical current through the unipolar system, and show how the coherent condensate fields respond to the current flow. The possibility of tailoring light via electrical current and vice versa simultaneously might lead to interesting new applications.

Table of Contents

List of Figures

Chapter 1

Introduction

In this chapter, I will breifly review the basic concepts of excitons and exciton-polaritons, followed by short surveys of these two closely connected fields. These surveys are not meant to be complete or anywhere near but just to outline the major developments of the two fields that shaped the modern understanding and paved the way for new progresses and explorations. The second part of this chapter reviews the physics of Bose-Einstein condensation (BEC). It summarizes the basic theoretical formulations of BEC of excitons and exciton-polaritons and points to review articles that cover extensively both experimental and theoretical works. These two parts serve mainly as a preparation for discussions in later chapters. In the last part, I will outline the orgnization of this thesis and briefly summarize each of the following chapters.

1.1 Basics and survey

1.1.1 Excitons

The basic concept of excitons can be understood in a simple two-level model in which the ground level with energy $-\epsilon$ is occupied (by an electron) while the excited level with energy $+\epsilon$ is empty. If one excites the electron by

transferring to it a finite energy $\Delta\epsilon = 2\epsilon$, it can be promoted directly to the excited level. One can think of this excited system as made up of an electron and an ion (or a "hole") with the latter being positively charged because the neutral ground state has lost a negative charge. Because both the electron and the hole have energy ϵ, the total energy becomes 2ϵ. This 2ϵ excitation could be resolved experimentally using, for example, absorption or emission spectroscopy.

However, this is often not the complete story of optical spectrum for a real system where Coulomb interaction plays a role. The excited electron feels the binding force from the ion or "hole" it left behind and the two can lower the total energy by forming a bound pair which is essentially a hydrogen-like atom in a renormalized sense. Like a hydrogen atom, this bound pair has a spectrum series $1s$, $2s$, $2p$, $3s$ and so on. Due to these bound states, the emission or absorption spectrum of the two-level system has not only the transition line mentioned above but also a series of hydrogenic lines with energy less than 2ϵ. These bound pairs are the so called "excitons".

The term *exciton* was first used by J. Frenkel in an effort to understand the energy transfer from optical excitations to vibrational modes in solids [33, 34]. In Frenkel's formulation, each atom of the solid crystal can, in the simplest case, be considered as a two-level system discussed above. The excitonic states localized on each atom are weakly coupled and the pair can hop between neighboring atoms. Shortly after J. Frenkel, another different but complementary understanding was proposed by G. Wannier [78] in terms

of the band structure picture. In his formulation, an exciton is a bound pair formed by an electron from the conduction band and a hole from the valence band. The pair carries a total momentum $\boldsymbol{K} = \boldsymbol{k}_e + \boldsymbol{k}_h$, which is the sum of electron and hole momentum.

These two formulations constitute our modern understanding of excitons (for detailed review see [51]). Frenkel excitons are bound pairs with orbital size smaller or comparable to the lattice spacing and exist in crystals of weakly bound atoms or molecules, for example, organic semiconductors, crystals formed by condensation of noble gases, some ionic crystals and etc [40, 51, 82]. On the other hand, Wannier excitons have their wavefunctions extended over many lattice cells. They exist mainly in semiconducting solid where the electron-hole interaction is substantially reduced by dielectric screening [40, 51, 82]. Throughout this thesis, we will be dealing with Wannier type excitons in conventional semiconductor quantum wells (QW) or in the newly discovered two-dimensional (2D) semiconductors, i.e. transition metal dichalcogenides (TMD).

Nearly two decades after Frenkel and Wannier's pioneering work, the field experienced a sharp rise in 1950s due to the increased interest in the optical properties of semiconducting solids [51]. Apart from the deviation in the shape of fundamental absorption edges predicted by the band theory, additional spectral lines traced to the excitonic states were observed lying next to the absorption edge. One of the earliest semiconductors studied and also the best known example of the existence of excitons is Cu_2O where sharp

absorption peaks of up to $n = 4$ hydrogenic levels were observed [7, 77]. The uncover of the intriguing optical property of Cu_2O triggered further expansion of the field of excitons into early 1960s [58]. Because of its strong Coulomb interaction (resulting in exciton binding energy of $\sim$ 150meV), Cu_2O turned into one of the major platforms for the search of exciton BEC [77] which I will review in the next section.

The next major development surged two decades later in 1980s when the growth and fabrication techniques of confined electronic systems such as semiconductor quantum wells and heterostructures had been developed. The increasing number of technological applications of their optoelectronic properties motivated extensive experimental investigations of excitons in lower dimensions [25, 49, 81]. These studies led people to realize that excitons play a much more important role in these systems than in bulk semiconductors because the confinement enhances the Coulomb interaction between electrons and holes and increases the oscillator strength.

1.1.2 Exciton-polaritons

Excitons and exciton-polaritons are closely connected in real systems because excitons carry electric dipole moments that couple easily with photons. To understand the concept of a polariton, recall the excited two-level system considered previously. The electron and the hole can only reside shortly in the bounded form before they collapse (so called radiative recombination process) and the system returns to its ground state. In this process, a photon with

the same energy as the exciton(i.e. $2\epsilon - \epsilon_b$ where ϵ_b is the exciton binding energy) is emitted. This photon could again create an exciton and the emission follows. These two processes could repeat in a time-periodic fashion, called Rabi oscillation, where energy is stored in an exciton for part of the period and in a photon for the rest of the period. The stationary version of this oscillating state is the *exciton-polariton* in which there is a finite probability for finding either an exciton or a photon at any particular time. In other words, polaritons are the eigenstate resulting from coupling of an exciton with a photon and their wavefunction are partly excitonic and partly photonic.

In a crystal environment, translational symmetry allows excitons to have well-defined momenta. For a bulk crystal, excitons with energy-momentum dispersion inside the light cone cannot exist on its own but couple with photon to form the lower and upper polariton states. When light enters the crystal, it turns into a polariton with same energy and transverse momentum (parallel to the crystal surface.)

The study of exciton-polaritons was pioneered by S. Pekar [62] and J. Hopefield [41] in the late 1950s. Alongside the development of the exciton field, two different theoretical approaches were developed to understand the light-matter coupling effect. The earlier theory of polaritons was based on second quantization formalism where both excitons and photons are quantized [41]. Later a semiclassical theory [12, 43]was also developed in which electromagnetic field are described by Maxwell's equation while the medium containing excitonic excitations are represented by frequency dependent dielectric func-

tions. These two approaches are equivalent in systems where nonlinear effect are negligible. The semiclassical approach is more complete in the sense that it could account for any possible nonlinear optical response.

A milestone in this field is the seminal discovery of exciton-polaritons in the vertical-cavity surface-emitting laser (VCSEL) by C. Weisbuch and coworkers [79]. A VCSEL consists of a quantum well sandwiched between two distributed Bragg reflectors where both excitons and photons are confined to two dimensions. Because the high finesse of their VCSEL, they were able to observe splittings of the reflection peak into lower and upper polariton branches and identify their findings as the strong coupling effect between excitons and photons. These branches are the so called *cavity-polaritons* and have since been the main subject of this field [2, 15, 70]. One of the major development afterwards was the realization of cavity-polariton BEC which will be discussed in next section.

1.2 Bose-Einstein condensation

Bose-Einstein condensation was proposed by S. Bose and A. Einstein in 1925 and first confirmed by the observation of superfluidity in liquid helium-4 in 1937. More than a half century later, it was realized in cold atom systems [1] thanks to the ground breaking development in the cooling technique. Although bosonic particles, e.g. excitons, polaritons and phonons, exist widely in condensed matter systems, BEC of these particles was not observed until the beginning of the twenty first century [48]. The fundamental difficulty lies

in the unstable nature of these quasiparticles which cannot live long enough for condensation to occur. However, it turns out that other than the unfavorably short lifetime, excitons and polaritons possess many outstanding properties that neither helium-4 nor gaseous atoms have. The possibility to tailor these bosons at will for potential new electronic and optoelectronic applications [53, 69] haven triggered enormous research efforts in overcoming their shortcomings and eventually led to convincing evidences of BEC of both excitons and exciton-polaritons.

1.2.1 Exciton condensation

Exciton BEC was first proposed by J. Blatt [10] and R. Casella [21] in early 1960s. Experimental search for exciton BEC began in 1970s with a focus on bulk semiconductors such as Cu_2O mentioned in previous section. For an extensive review on bulk exciton BEC see for example [72]. Bearing the same fate as bulk exciton case, the quest for BEC in semiconductor quantum wells is also limited by the too short lifetime of excitons for example in GaAs quantum wells. The radiative recombination process prevents the formation of low temperature thermal equilibrium state.

In 1970s, Y. Lozovik and V. Yudson [54] proposed the idea of *spatially indirect excitons* as a way to overcome this obstacle. In their proposal, electrons and holes are spatially separated in different quantum wells which greatly suppresses the recombination process. The basic physical picture of BEC remains valid in the indirect case. This approach has been tested by many

experimental efforts in since 1990s and despite the ongoing debate whether the observed coherence is sufficient to proof the realization of BEC, it has tremendously advanced and deepened our understanding of the nature of exciton BEC. For a detailed review on the progress of indirect exciton condensation, I suggest the recent review article [23].

Now we briefly summarize the theoretical formalism that has been developed for the description of exciton condensation [18,24,46,83,89]. It is based on BCS-like mean-field theory in which the ground state can be described by a coherent state wavefunction

$$|\phi_G\rangle = \Pi_{\boldsymbol{k}}[u_{\boldsymbol{k}} + v_{\boldsymbol{k}}\hat{a}^\dagger_{\boldsymbol{k},c}\hat{a}_{\boldsymbol{k},v}]|0\rangle \tag{1.1}$$

where $\hat{a}_{\boldsymbol{k},c}$ and $\hat{a}_{\boldsymbol{k},v}$ are annihilation operators for conduction band and valence band electrons respectively. $|0\rangle$ is the vacuum state in which the conduction band is empty and valence band is fully occupied. The Hamiltonian of the interacting system is

$$\hat{H} = \sum_{\boldsymbol{k},\alpha}\epsilon_\alpha(\boldsymbol{k})\hat{a}^\dagger_{\boldsymbol{k},\alpha}\hat{a}_{\boldsymbol{k},\alpha} + \frac{1}{2A}\sum_{\boldsymbol{q},\boldsymbol{k}_1,\boldsymbol{k}_2} V(\boldsymbol{q})\hat{a}^\dagger_{\boldsymbol{k}_1+\boldsymbol{q},\alpha}\hat{a}^\dagger_{\boldsymbol{k}_2-\boldsymbol{q},\beta}\hat{a}_{\boldsymbol{k}_2,\beta}\hat{a}_{\boldsymbol{k}_1,\alpha} \tag{1.2}$$

where $\alpha = c, v$ is the band indices and $\epsilon_{c(v)}(\boldsymbol{k}) = \pm\epsilon_{\boldsymbol{k}}$ the single particle energy dispersion. $V(\boldsymbol{q})$ is the Fourier transform of Coulomb interaction which is often replaced by the renormalized version to account for dielectric screening. By minimizing the energy of the variational wavefunction,

$$E = \langle\phi_G|\hat{H} - \mu\hat{n}_{\rm ex}|\phi_G\rangle \tag{1.3}$$

a set of coupled mean-field equations could be obtained:

$$\xi_{\boldsymbol{k}} = \epsilon_{\boldsymbol{k}} - \mu - \sum_{\boldsymbol{k}'} V(\boldsymbol{k}-\boldsymbol{k}')(1 - \xi_{\boldsymbol{k}'}/E_{\boldsymbol{k}'}), \tag{1.4}$$

$$\Delta_{\boldsymbol{k}} = \sum_{\boldsymbol{k}'} V(\boldsymbol{k}-\boldsymbol{k}')\Delta_{\boldsymbol{k}'}/E_{\boldsymbol{k}'}, \tag{1.5}$$

$$E_{\boldsymbol{k}}^2 = \xi_{\boldsymbol{k}}^2 + \Delta_{\boldsymbol{k}}^2. \tag{1.6}$$

By self-consistently solving these coupled equations, the coefficient of $u_{\boldsymbol{k}}$ and $v_{\boldsymbol{k}}$ can be obtained as a function of the chemical potential μ. The behavior of the solution has been discussed by several works which will not be repeated here. This formalism has also been used in the discussion of BEC-BCS crossover where the density of excitons varies from the dilute limit, $n_{\rm ex}a_B^2 \ll 1$, to the dense, $n_{\rm ex}a_B^2 \sim 1$ limit. In this thesis, we will mainly focus on the dilute limit where the coherence coefficient can be simply approximated by

$$u_{\boldsymbol{k}} = \frac{1}{\sqrt{1+\lambda_0^2\phi_{\boldsymbol{k}}^2}} \approx 1 \tag{1.7}$$

$$v_{\boldsymbol{k}} = \frac{\lambda_0\phi_{\boldsymbol{k}}}{\sqrt{1+\lambda_0^2\phi_{\boldsymbol{k}}^2}} \approx \lambda\phi_{\boldsymbol{k}} = \phi_{\boldsymbol{k}}\sqrt{n_{ex}} \tag{1.8}$$

where $\lambda_0 \equiv \sqrt{n_{\rm ex}}$ and $\phi_{\boldsymbol{k}}$ is the momentum representation of the hydrogenic wavefunction

1.2.2 Exciton-polariton condensation

Exciton-polaritons in bulk semiconductors have no minimum in their energy dispersion where macroscopic occupation can occur. Experiments on exciton-polariton BEC only began after the strong coupling regime was realized in VCSEL as mentioned in previous section. The first experimental

observation of exciton-polariton BEC was made by J. Kasprzak and coworkers on CdTe based QW-microcavity system [48]. A series of review articles have been published over the past few years where detailed review on this field are provided [19, 20, 26, 53, 69].

BEC of exciton-polaritons can also be treated using a BCS-like mean field theory. The crucial difference here is the inclusion of the coherent photon field in the ground state wavefunction which could be written as:

$$|\phi_G\rangle = \exp(\lambda \hat{a}^\dagger_{\rm ph} - \lambda^2/2)\Pi_{\boldsymbol{k}}[u_{\boldsymbol{k}} + v_{\boldsymbol{k}}\hat{a}^\dagger_{\boldsymbol{k},c}\hat{a}_{\boldsymbol{k},v}]|0\rangle \tag{1.9}$$

where $\hat{a}^\dagger_{\rm ph}$ is the creation operator of cavity photons. $\lambda = \sqrt{n_{\rm ph}}$ parametrizes the photon density. $|0\rangle$ is also generalized to mean the vacuum of photons. The coefficient $u_{\boldsymbol{k}}$ and $v_{\boldsymbol{k}}$, the photon density $n_{\rm ph}$ and the chemical potential μ can be determined self-consistently using a set of extended mean field equations. I will not repeat the details of this calculation but only remark that the presence of the photon field enhances the coherence between the conduction and the valence band states.

On a macroscopic level, exciton-polariton condensates can be described by the coupled Gross-Pitaevskii equations [63],

$$\frac{\partial \psi_{\rm ex}}{\partial t} = -\frac{\hbar^2\nabla^2}{2m_{\rm ex}}\psi_{\rm ex} + \frac{\hbar\Omega_{\rm R}}{2}\psi_{\rm ph} + g|\psi_{\rm ex}|^2\psi_{\rm ex} \tag{1.10}$$

$$\frac{\partial \psi_{\rm ph}}{\partial t} = -\frac{\hbar^2\nabla^2}{2m_{\rm ex}}\psi_{\rm ph} + \frac{\hbar\Omega_{\rm R}}{2}\psi_{\rm ex} \tag{1.11}$$

where g is the exciton-exciton interaction strength and $\Omega_{\rm R}$ is the Rabi oscillation frequency. These basic equations have also been developed to account for the dynamic effects of pump and decay in the polariton steady states.

1.3 Structure and outline

The bulk of this thesis is a collection of our works based on exciton and exciton-polariton condensates and is organized as follows.

The second chapter presents our theory of coherent two-particle tunneling mechanism in exciton condensate state. We start from the mean-field theory of exciton condensate introduced in previous section and develop a theory of the two-particle tunneling process based on second order perturbation theory. It is then applied to a vertically stacked heterostructure based on monolayers of graphene and transition-metal dichalcogenides (TMD) double layer. Later a simple analytical result is obtained for the two-particle tunneling conductance at low exciton density limit. In the second half of the chapter, we propose both *dc* and *ac* electric measurements based on this mechanism and discuss the current-voltage response characteristic where crucial information of exciton condensates could be extracted.

The third chapter expands the theory of the two-particle tunneling mechanism to non-condensate cases and proposes a thermoelectric cooling device based on this theory. We first develop the theory of two-particle tunneling for excitons with a quasi-thermal equilibrium population. A four-contact cooling device is then proposed where electric current is converted to exciton current which extracts heat from one end of the device and deposit it on the other end. We discuss different bias scenarios for controlling the direction of flow of this exciton current.

In the fourth chapter, we propose a way to generate exciton or exciton-polariton supercurrents electrically. We start by introducing a unipolar (specifically $n-i-n$) device, in which the intrinsic part is embedded in a semiconductor microcavity and hosts a polariton condensate supported by continuous external laser pump. Under mean-field approximation, we solve the scattering problem between the non-interacting region (n) and the coherent region (i) and discuss the spatial dependence of the currents which indicates a induced supercurrent. A two step model is introduced to illustrate the process for the conversion of the induced exciton supercurrent near the interface to the polariton supercurrent in the bulk region. We then calculate the current-voltage relation based on the Landauer-Büttiker formalism assuming ballistic quasiparticle transport. In the last part, we show the possibility of detecting this superflow in a microcavity set up where photons that leak out the cavity carry a finite transverse momentum and discuss its promising potential for new applications in opto-electronic devices.

Chapter 2

Electrical reservoirs for spatially indirect excitons

2.1 Introduction

Excitons are composite bosonic particles in which conduction band electrons bind with valence band holes. Excitons normally exist as excited states of semiconductors and insulators, but can have extremely long lifetimes when the electron and hole are separated in momentum-space, or in real-space [54], or both. Bose-Einstein condensation of long-lived excitons was predicted several decades ago, [50] and is thought to have been realized relatively recently in semiconductor quantum well [16, 17, 37–39] double layers. Closely related polariton condensate states, in which longer range coherence is assisted by the small masses of two-dimensional vertical cavity photons, are regularly realized and have been studied extensively over the past decade [5, 6, 19, 20, 26, 29, 48, 69, 71, 74, 80]. In typical exciton-condensation experiments a population of electrons and holes is generated in nearby 2D layers by optical excitation. Free electrons and holes can also be injected electrically if contacts can be established to conduction and valence bands. The electrons and holes then combine to form excitons and the excitonic state is revealed by photons emitted during the exciton radiative decay process. [1]In this paper

we propose and theoretically analyze an electrically-controlled mechanism applicable to the case 2D material double layers in which excitons are generated directly and discuss some of its potential advantages.

In recent years 2D transition metal dichalcogenide (TMD) semiconductors have been established as an exciting exciton physics platform [56, 64] in which energy scales are enhanced by strong Coulomb interactions. Surprising flexibility in the design of optical and opticalelectronic properties can be achieved [35, 57, 60] by stacking van der Waals (vdW) coupled 2D materials in a variety of different arrangements. vdW heterojunctions involving 2D semiconductors can host spatially indirect excitons formed from electrons and holes in two different layers. Because Coulomb interactions are strong, the binding energy of these spatially indirect excitons remain strong even when the electron and hole layers are separated by hexagonal boron nitride (hBN) layers that increase exciton lifetimes by orders of magnitude from the nanosecond [61, 66] range that applies in the absence of spacer layers. The tunable and exceptionally long lifetime of spatially indirect excitons in vdW heterojunctions expands the range of physics that can be explored using the exciton reservoirs described in this paper.

Our theory of electrical reservoirs for excitons is based on a fermionic mean-field theory of the exciton condensate state. [24, 83, 89] In the fermionic mean field theory of a spatially indirect double layer condensate, quasiparticle

[1]For systems in which dark excitons (excitons with momentum or spin quantum numbers that don't match photons) are favored however, direct optical access is blocked.

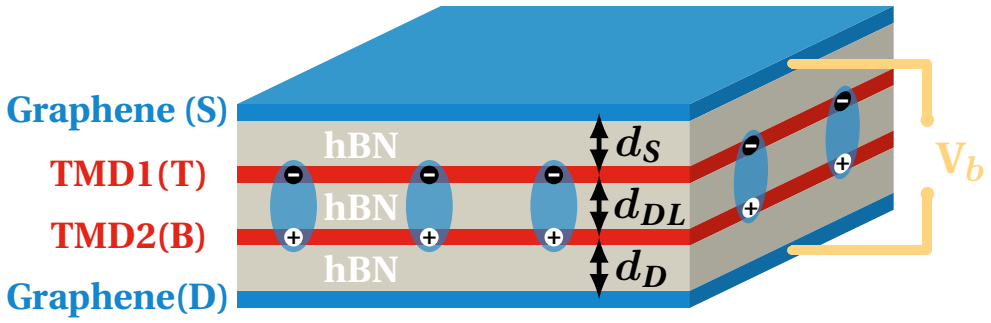

Figure 2.1: (Color online) Schematic illustration of a 2D material heterojunction capable for supporting a spatially indirect exciton condensate, and of an electrode pair that can act as a reservoir for spatially indirect excitons.

energies are altered by the interlayer coherence that the condensate establishes and the energy gap is enhanced. Electrons or holes in an electrode that have an energy inside this gap cannot tunnel into quasiparticle states of the double layer. However, we find that because of the Coulomb interaction and the exciton binding energy it produces, correlated pair tunneling from electrodes connected to the two different layers is possible. In this paper, we develop a microscopic model of this two particle tunneling process and argue that electrode pairs that act as exciton reservoirs have many advantages over other exciton generation and control strategies.

2.2 Excitonic crossed Andreev tunneling

We consider the vertically stacked multilayer heterostructure system illustrated in Fig. 2.1 which contains a TMD semiconductor double layer (DL) that hosts spatially indirect exciton states, two layers above and below the

semiconductor double layer that act as source (S) and drain (D) electrodes, and hBN tunnel barrier layers of variable thickness. For the sake of definiteness we will assume below that the electrodes consist of single layer graphene, which has the advantage of being gapless, but this detail is inessential. The graphene electrodes could be substituted by any 2D or bulk conducting material without substantial consequence. We assume that the TMD double layer has a spatially indirect gap between the conduction band of its top (T) layer and the valence band of its bottom (B) layer (See Fig. 2.2a), due either to the natural band alignment of the 2D materials or to an electric field established across the entire structure by a gate voltage. Finally we assume that the chemical potentials of the reservoirs lie outside of the 2D material bands, and that an external bias voltage maintains the chemical potential difference between the source and the drain electrodes, $\mu_S - \mu_D = eV_b$ at a value smaller than the spatially indirect band gap. Here $e > 0$ is the magnitude of the electron charge. Under these circumstances, the ground state of double layer does not contain any free fermionic quasiparticles, but it will contain excitons when eV_b is larger than the energy needed to create a spatially indirect exciton. To explain our main idea we concentrate here on the case of $T = 0$ for which the excitons form a 2D XY condensate. The main idea of using an electrode pair as a reservoir for excitons applies equally well when the excitons form a non-condensed gas.

The total Hamiltonian of the four-layer system is

$$\hat{\mathcal{H}} = \hat{\mathcal{H}}_S + \hat{\mathcal{H}}_D + \hat{\mathcal{H}}_{DL} + \hat{\mathcal{H}}_t. \tag{2.1}$$

The graphene electrode Hamiltonians are

$$\hat{\mathcal{H}}_\alpha = \sum_{\bar{\boldsymbol{p}}} \epsilon^\alpha_{\bar{\boldsymbol{p}}}\, \hat{a}^\dagger_{\bar{\boldsymbol{p}},\alpha} \hat{a}_{\bar{\boldsymbol{p}},\alpha} \tag{2.2}$$

where $\alpha = S, D$. In Eq. 2.2 $\bar{\boldsymbol{p}} \equiv (\boldsymbol{p}, \lambda, \tau)$ is a compound index that combines 2D momentum $\boldsymbol{p}$, band index $\lambda = c, v$ for the positive and the negative branches of the Dirac cone and valley index τ for the K and K' valleys. [2] $\hat{a}^\dagger_\alpha$ and $\hat{a}_\alpha$ are electron creation and annihilation operators in the electrodes.

The interacting Hamiltonian of the double layer TMD is

$$\hat{\mathcal{H}}_{DL} = \sum_{\boldsymbol{k},\beta} \epsilon^\beta_{\boldsymbol{k}} \hat{c}^\dagger_{\boldsymbol{k},\beta} \hat{c}_{\boldsymbol{k},\beta} + \frac{1}{2A} \sum_{\beta,\beta'} \sum_{\boldsymbol{q},\boldsymbol{k},\boldsymbol{k'}} V_{\beta\beta'}(\boldsymbol{q}) \hat{c}^\dagger_{\boldsymbol{k}+\boldsymbol{q},\beta} \hat{c}^\dagger_{\boldsymbol{k'}-\boldsymbol{q},\beta'} \hat{c}_{\boldsymbol{k'},\beta'} \hat{c}_{\boldsymbol{k},\beta} \tag{2.3}$$

where $\beta, \beta' = T, B$ and $\hat{c}^\dagger_{T(B)}$ are creation operators for conduction band electrons in the top layer (valence band electrons in the bottom layer) of the double-layer TMD. $V_{\beta\beta'}(\boldsymbol{q}) = 2\pi e^2 e^{-|\boldsymbol{q}|d_{\beta\beta'}}/(\epsilon|\boldsymbol{q}|)$ is the Coulomb interaction potential, where the diagonal components $d_{\beta\beta}$ are zero and the offdiagonal components $d_{TB} = d_{BT} \equiv d_{DL}$ denotes the interlayer spacing of the double-layer TMD. ϵ is the dielectric constant of hBN. Note that we have retained only one band in each TMD layer because the other bands are separated energetically and don't contribute to the tunneling process.

[2] The spin degree of freedom has been ignored in our model for two reasons: (1) The spin splitting in the conduction bands of TMD monolayers is small and the relative order of spin-up and spin-down bands depends on material. (2) According to mean field theory [83], the excitonic ground state consists of separate condensates for the two-different spin components. To avoid these complications, we drop the spin degree for simplicity while focusing on the microscopic tunneling model. Spin can be added without any change in the basic idea when modeling the physics we discusss in particular materials.

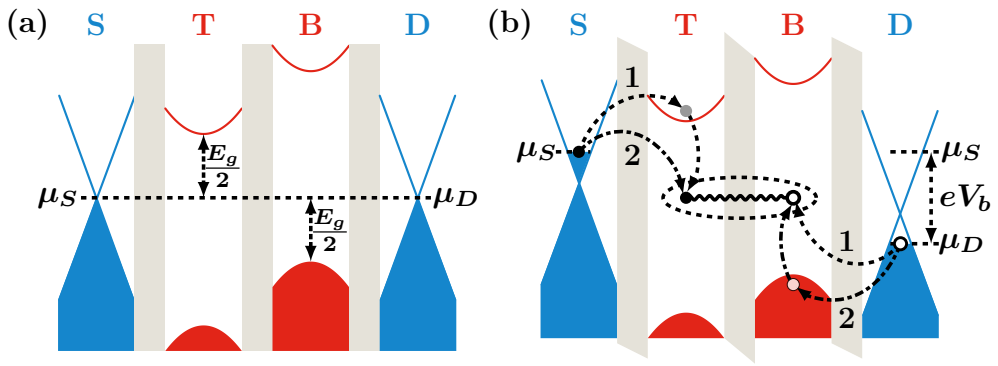

Figure 2.2: (Color online) Schematic band diagrams for the vertical vdW heterostructure systems of interest for the case of (a) zero applied bias and (b) a finite bias with $E_g > V_b > \mu_{ex0}$. (μ_{ex0} is the excitation energy of a single isolated exciton.) At zero bias (a), we assume for definiteness that the Dirac points of the electrodes align with the middle of the spatial indirect band gap. When $V_b < \mu_{ex}$, the electrodes become charged, which induces band bending across the heterostructure but no tunneling occurs. In case (b), electrons (filled black circle) and holes (empty circles) start to tunnel into the virtual states (filled gray and pink circles) in the TMD double layer, and couple to form excitons as indicated by the dashed and dash-dotted arrows. The labels 1 and 2 distinguish the two processes with virtual intermediate states containing electrons in the top layer conduction band from those containing holes in the bottom layer valence bands that are described in detail in the main text.

Electron tunneling between the electrodes and the double layer system is described by the Hamiltonian

$$\hat{\mathcal{H}}_t = \sum_{\boldsymbol{k},\bar{\boldsymbol{p}}} t^S_{\boldsymbol{k}\bar{\boldsymbol{p}}}\, \hat{c}^\dagger_{\boldsymbol{k},T} \hat{a}_{\bar{\boldsymbol{p}},S} + t^D_{\boldsymbol{k}\bar{\boldsymbol{p}}}\, \hat{c}^\dagger_{\boldsymbol{k},B} \hat{a}_{\bar{\boldsymbol{p}},D} + h.c. \tag{2.4}$$

where $t^{S(D)}_{\boldsymbol{k}\bar{\boldsymbol{p}}}$ is a tunneling matrix element. Note that the assumption that momentum is not conserved upon tunneling is inessential. For single-grain hBN tunnel barriers, the tunneling properties can have very specific momentum dependence that is sensitive to the relative orientation of the various 2D material layers, but is not accounted for below. We also neglect interlayer tunneling between the two TMD layers primarily because we are interested in a bias voltage regime in which free carriers are not present to tunnel. (We elaborate on this point later.) We also set the interlayer radiative recombination rate to zero in order to focus on double-electrode reservoir properties. In practice we anticipate that the interplay between our exciton reservoirs and interlayer radiative recombination, whose strength can be adjusted over orders of magnitude by varying the hBN barrier thickness and orientation, opens up a rich range of opto-electronic phenomena for study that are collectively the primary motivation for this work.

The band diagram of the vertical vdW heterostructure system is shown schematically in Fig. 2.2. At zero bias (Fig. 2.2a), we assume both graphene electrodes are neutral and that their Dirac points align with the middle of the spatially indirect band gap E_g. Note that $E_g \equiv E_g(V_b)$ varies as a function of bias voltage because of charge accumulation in the electrodes. When a bias

voltage in the subgap regime ($E_g > V_b > 0$) is applied, tunneling between the electrodes and free-carrier states in the TMD layers is prohibited by energy conservation. Direct tunneling of electrons from the source to the drain is also strongly suppressed because it must overcome three tunneling barriers. One can enable normal tunneling by increasing the bias voltage so that it exceeds the indirect band gap ($V_b > E_g$). In this case, electrons with high enough energy could tunnel directly to the TMD layer and interlayer-intraband tunneling between the TMD layers becomes possible. Consequently, electrons can tunnel from the source to the drain via three consecutive first order tunneling processes.

Our interest here however is in the bias regime $E_g > V_b > \mu_{ex0}$, where μ_{ex0} is the energy of an isolated spatially indrect exciton. In this bias voltage regime energy conservation is can be achieved by moving an electron from the top electrode to the top layer, and from the bottom layer to the bottom electrode, while adding a spatially indirect exciton to the TMD double layer. Below we calculate the rate of this second order process that involves two tunneling steps as illustrated in Fig. 2.2b. The state created when an electron from the source tunnels to a virtual state in the top layer and a hole from the drain subsequently tunnels to the bottom layer has a finite overlap with a state in which a spatially indirect exciton is added to the double-layer system. An alternative and equally possible path is for a hole from the drain tunnels to tunnel to a virtual state in the bottom layer first, followed by an electron which tunnels into the top layer and combines with the hole to form a bound

exciton. This process is analogous to crossed Andreev reflection (CAR, also known as non-local Andreev reflection) in a normal metal-superconductor-normal metal (NSN) junction [14]. In that case an electron injected from the source is effectively reflected as an electron in the drain, whereas in the NSN junction case a hole is reflected generating a spatially indirect exciton in the double-layer TMD.

One important aspect of modeling this tunneling process is the thermodynamics of the excitons. It is well known that excitons can undergo a BKT phase transition to condensed phase as the temperature is lowered or as the density is increased. Here we focus on $T < T_{\mathrm{BKT}}$ because it is more interesting, and yet simpler. We find that because of the stimulated scattering characteristic of bosonic statistics, a major fraction of the excitons added or removed from the system and simply added or removed from the condensate.

The condensate state of spatially indirect excitons has been well studied previously in several works [24, 83, 89] using BCS-like mean field theory approach where the ground state is found by minimizing $\langle \hat{\mathcal{H}}_{DL} - \mu_{ex}\hat{\mathcal{N}} \rangle$ where $\hat{\mathcal{N}} = \sum_{\boldsymbol{k}} (\hat{c}^{\dagger}_{\boldsymbol{k},T}\hat{c}_{\boldsymbol{k},T} + \hat{c}_{\boldsymbol{k},B}\hat{c}^{\dagger}_{\boldsymbol{k},B})/2$ are the total electron-hole number. The total energy of the exciton condensate system takes the form

$$E = E_G + \sum_{\boldsymbol{k}} E_{\boldsymbol{k}} (\hat{\gamma}^{\dagger}_{\boldsymbol{k},0}\hat{\gamma}_{\boldsymbol{k},0} - \hat{\gamma}^{\dagger}_{\boldsymbol{k},1}\hat{\gamma}_{\boldsymbol{k},1}) + \mu_{ex}\hat{\mathcal{N}} \tag{2.5}$$

where E_G is the condensate ground state energy and μ_{ex} the exciton chemical potential. The quasiparticle energy dispersion is $E_{\boldsymbol{k}} = \sqrt{(\epsilon^T_{\boldsymbol{k}} - \mu_{ex}/2)^2 + \Delta^2_{\boldsymbol{k}}}$, where we have assumed $\epsilon^T_{\boldsymbol{k}} = -\epsilon^B_{\boldsymbol{k}}$ and the order parameter $\Delta_{\boldsymbol{k}}$ is real and

negligible for the case of low exciton density. $\hat{\gamma}^\dagger_{\boldsymbol{k},0} = u_{\boldsymbol{k}}\hat{c}^\dagger_{\boldsymbol{k},T} + v_{\boldsymbol{k}}\hat{c}^\dagger_{\boldsymbol{k},B}$ and $\gamma^\dagger_{\boldsymbol{k},1} = v_{\boldsymbol{k}}\hat{c}^\dagger_{\boldsymbol{k},T} - u_{\boldsymbol{k}}\hat{c}^\dagger_{\boldsymbol{k},B}$ are creation operators for states in the empty and the occupied quasiparticle bands, respectively. $u_{\boldsymbol{k}}$ and $v_{\boldsymbol{k}}$ are the coherence factors obtained self-consistently in the mean field theory.

The two particle (or the excitonic crossed Andreev) tunneling rate can be obtained using Fermi's golden rule to the second order in $\mathcal{H}_t$,

$$\frac{dn_{ex}}{dt} = \frac{2\pi}{\hbar A}\sum_{\bar{\boldsymbol{p}},\bar{\boldsymbol{p}}'} |M_{\bar{\boldsymbol{p}}\bar{\boldsymbol{p}}'}|^2 \,(f^S_{\bar{\boldsymbol{p}}} - f^D_{\bar{\boldsymbol{p}}'})\delta(\epsilon^S_{\bar{\boldsymbol{p}}} - \epsilon^D_{\bar{\boldsymbol{p}}'} - \mu_{ex}) \tag{2.6}$$

where n_{ex} is the exciton density and A the cross-sectional area of the heterostructure. $f^\alpha_{\bar{\boldsymbol{p}}}$, where $\alpha = S, D$, is the Fermi distribution function which we approximate by the zero temperature form $f^\alpha_{\bar{\boldsymbol{p}}} = \Theta(\mu_\alpha - \epsilon^\alpha_{\bar{\boldsymbol{p}}})$, where $\Theta(x)$ is the Heaviside function. The matrix element takes the form

$$M_{\bar{\boldsymbol{p}}\bar{\boldsymbol{p}}'} = \sum_{\boldsymbol{k}} u_{\boldsymbol{k}} v_{\boldsymbol{k}} t^S_{\boldsymbol{k}\bar{\boldsymbol{p}}} t^{D*}_{\boldsymbol{k}\bar{\boldsymbol{p}}'} \left\{ \frac{1}{E^0_{\boldsymbol{k}} - \epsilon^S_{\bar{\boldsymbol{p}}}} + \frac{1}{\epsilon^D_{\bar{\boldsymbol{p}}'} - E^1_{\boldsymbol{k}}} \right\} \tag{2.7}$$

where $E^0_{\boldsymbol{k}} = E_{\boldsymbol{k}} + \mu_{ex}/2$ and $E^1_{\boldsymbol{k}} = -E^0_{\boldsymbol{k}}$ are the energies required for adding an quasiparticle of momentum $\boldsymbol{k}$ in the quasiparticle bands 0 and 1 respectively. The energy denominators reflect the finite energy cost for hopping to the intermediate virtual states. The two terms in the matrix elements accounts for the two paths of tunneling depicted in Fig. 2.2b.

Evaluation of the matrix element $|M_{\bar{\boldsymbol{p}}\bar{\boldsymbol{p}}'}|^2$ in Eq. (2.7) requires the knowledge of the momentum dependence of $t^\alpha_{\boldsymbol{k}\bar{\boldsymbol{p}}}$. (Ming: I'm not very clear here.) In the weak tunneling regime, interfacial disorder plays an important role in determining the tunneling amplitude. Here, without going into details,

we employ a Gaussian random tunneling model to describe the tunneling amplitudes, which assumes that $\langle t^{\alpha}(\boldsymbol{r})\rangle_{\rm dis} = 0$ and the second order correlation functions

$$\langle t^{\alpha}(\boldsymbol{r}) t^{\alpha'*}(\boldsymbol{r})\rangle_{\rm dis} = |\Delta t|^2 \mathcal{F}(\boldsymbol{r}-\boldsymbol{r}')\delta_{\alpha\alpha'} \tag{2.8}$$

where $\langle\cdots\rangle_{\rm dis}$ is the disorder average and $\mathcal{F}(\boldsymbol{r}-\boldsymbol{r}')$ is a smooth decaying function of the distance $\boldsymbol{r}-\boldsymbol{r}'$. In the low exciton condensate density limit, we obtain the tunneling current-voltage equation

$$I_{ex} \approx G_{ex}(V_b - \mu_{ex}/e) \tag{2.9}$$

where the tunneling conductance is

$$G_{ex} = \frac{A g_N^S g_N^D n_{ex} a_B^2}{e^2/\hbar}\frac{8}{\rho_0 E_b} \tag{2.10}$$

where g_N^S and g_N^D are the normal tunneling conductancea per unit area between the source and the top layer and between the drain and the bottom layer, respectively. ρ_0 is the density of states of the quasiparticle band 0. a_B is the Bohr radius and E_b the exciton binding energy. The resulting tunneling conductance Eq. (2.10) is proportional to the exciton condensate density n_{ex} due to the well-known bosonic stimulated scattering. Because of this final state effect, the possibility that the two-particle tunneling process creates excitons with energy above the condensate ground state is significantly suppressed. Since even in the low density BEC limit of condensation the fraction of uncondensed excitons is small, in deriving the above result we assumed that

the contributions from processes with a final state exciton outside the condensate are negligible. By taking $g_N^S = g_N^D \sim 10^{-2} e^2/h \cdot \mu m^{-2}$, $n_{ex} a_B^2 \sim 0.01$ and effective mass of quasiparticle bands in TMD layers to be the bare electron mass, we estimate that G_{ex}/A is in the order $10^{-11} e^2/h \cdot \mu m^{-2}$.

Eq. (2.9) shows explicitly the threshold condition for the two-particle tunneling process to occur, which is $eV_b > \mu_{ex}$. The seemingly linear current voltage relation, however, doesn't lead to a steady state current because as n_{ex} increases, μ_{ex} also increases until it reaches the equilibrium value $eV_b = \mu_{ex}$ at which the current vanishes. This will be discussed in detail in next section, where we study the electrostatic properties of the equilibrium state.

2.3 Electrostatics of the equilibrium state

Because of the interacting nature of excitons, μ_{ex} varies as more excitons are injected into the condensate. Mean field theory [83] predicts that, for low exciton densities, the change in μ_{ex} caused by exciton-exciton interaction is $\Delta\mu_{ex} = (g_H + g_X) n_{ex}$, where the g_H and g_X represent the Hartree and the Fock coupling strengths, respectively. The Hartree term $g_H = e^2/C_{DL} = \epsilon/(4\pi d_{DL})$ accounts for the capacitive coupling between the top and the bottom layers, where C_{DL} is the capacitance of the TMD double layer. The exchange coupling term originates from both intralayer and interlayer Coulombic exchange interactions and thus depends on the interlayer spacing d_{DL} as well. Taking into account the electrostatic potential energy caused by the charged electrodes,

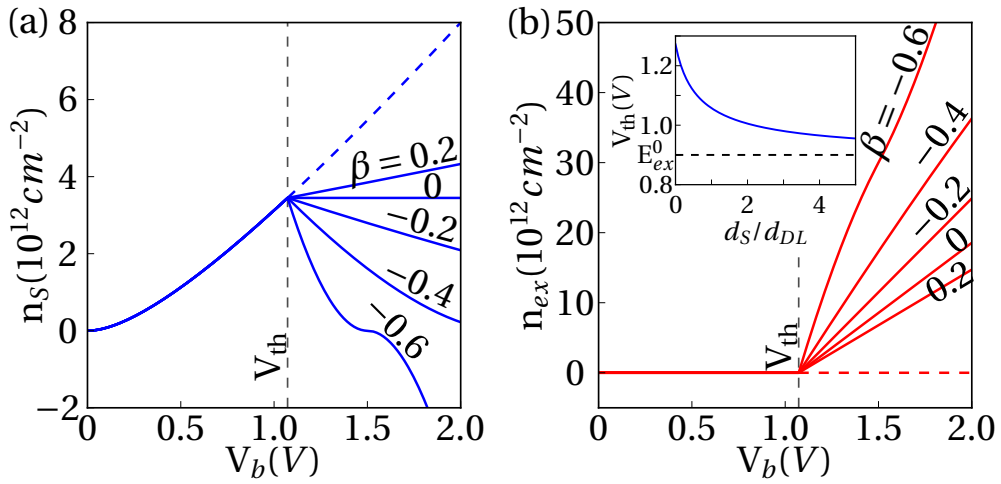

Figure 2.3: Equilibrium state source densities (a) and exciton densities (b) at different relative ratios of the Fock to the Hartree coupling strengths $\beta = g_X/g_H$, where $g_H = \epsilon/(4\pi d_{DL})$ is fixed with its value set by $d_{DL} = 1nm$. The result is obtained by assuming a symmetric structure $d_S = d_D$ and choosing $d_S/d_{DL} = 1$, $E_g = 1.1eV$ and $E_b = 0.2eV$. The extended (colored) dashed line represent densities in the case where excitons are absent. The vertical gray dashed lines indicate threshold voltage. Inset: Threshold voltage as a function of d_S/d_{DL} where the dashed line indicates the zero density limit exciton energy E^0_{ex}.

the total chemical potential is

$$\mu_{ex} = E^0_{ex} + (g_H + g_X)n_{ex} + g_H n_S \tag{2.11}$$

where $E^0_{ex} = E_g(0) - E_b$ and n_S is the electron density in the source and assumed to be equal to the hole density n_D in the drain. We see that at μ_{ex} grows linearly as increasing n_{ex} and n_S, and an equilibrium state can be reached when $eV_b = \mu_{ex}$.

At equilibrium, the total energy density of the system is found to be

$$\begin{aligned}\mathcal{E}(n_S, n_{ex}) =& E^0_{ex} n_{ex} + \frac{1}{2} g_H (n_S + n_{ex})^2 + \frac{1}{2} g_X n_{ex}^2 \\ &+ \frac{4\sqrt{2\pi}\hbar v}{3e^2} |n_S|^{3/2} + \frac{2\pi e^2 (d_S + d_D) n_S^2}{\epsilon} \\ &- eV_b(n_S + n_{ex})\end{aligned} \tag{2.12}$$

where the last term acts as a Lagrange multiplier. Minimizing $\mathcal{E}$ leads to

$$\frac{n_{ex}}{C_{DL}} + n_S \left(\frac{2\hbar v\sqrt{2\pi}}{e^2\sqrt{|n_S|}} + \frac{1}{C_{geo}} \right) = V_b \tag{2.13}$$

and the equilibrium condition $eV_b - \mu_{ex} = 0$. Eq. (2.13) recovers the usual capacitor circuit equation, where $C_{geo} = 4\pi e^2 d_{tot}/\epsilon$ is the total geometric capacitance of the heterostructure, where $d_{tot} = d_S + d_{DL} + d_D$. In solving for the energy minimum, we required that $n_{ex} \geq 0$.

Fig. 2.3 shows the equilibrium densities for several typical values of the Fock coupling strength $\beta = g_X/g_H$ relative to fixed g_H. For V_b below the threshold voltage V_{th}, which is determined by $eV_{\text{th}} = E_g(V_{\text{th}}) - E_b$, no exciton is injected and n_S increases independently of β with increasing V_b. When

$V_b > V_{\rm th}$, electrons and holes can enter the TMD layers by forming excitons via the crossed Andreev tunneling process. Because part of the electron and the hole densities are sucked into the exciton state, the overall slope of the n_S curve is reduced and becomes negative when β changes sign from positive to negative. For $\beta < 0$, we found that the source (drain) becomes positively (negatively charged), i.e. $n_S < 0$, at $V_b = -E^0_{ex}/\beta$, where distinct behavior in the dynamic response occurs as we will discuss later in Sec. 2.4. The parameter β is taken as an input parameter in our model. For comparison, $\beta = -0.6$ corresponds to the value found for $d_{DL} = 1nm$ in the self-consistent mean field calculation Inset of Fig. 2.3b plots $V_{\rm th}$ as the ratio of the thicknesses d_S/d_{DL} is varied.

Because of the opposite trends in n_S and n_{ex} for $\beta < 0$, according to Eq. (2.11), it is possible that the increase in μ_{ex} due to the exciton-exciton interaction is less than the decrease in the band bending $g_H n_S$ due to the charged electrodes. In this situation, μ_{ex} decreases as more excitons are injected, implying possible instabilities in the system.

To understand the stability of the system, we calculate the second order variation $\delta^{(2)}\mathcal{E}$ due to small variations in n_S and n_{ex}. The local stability requires that $\delta^{(2)}\mathcal{E} > 0$ which translates to

$$\frac{\partial^2 \mathcal{E}}{\partial n_S^2} \cdot \frac{\partial^2 \mathcal{E}}{\partial n_{ex}^2} - \left(\frac{\partial^2 \mathcal{E}}{\partial n_S \partial n_{ex}} \right)^2 > 0. \tag{2.14}$$

It leads to the condition $(1+\beta)\gamma > 1$, where $\gamma \equiv (1 + 2C_{geo}/C_Q) d_{tot}/d_{DL}$ and $C_Q = \sqrt{2n_S}/(\sqrt{\pi}\hbar v)$ is the quantum (differential) capacitance of graphene [85]

ignoring spin degeneracy. We found that a global minimum exists irrespective of V_b for $(1+\beta)d_{tot}/d_{DL} > 1$. Given $d_S = d_{DL} = d_D$, this global stability condition corresponds to $\beta > -2/3$ which contains all the cases plotted in Fig. 2.3. For the regime $(1+\beta)d_{tot}/d_{DL} < 1$, there is a finite bias range where $\mathcal{E}$ has a local minimum existing between two saddle points. Beyond this bias range, the local minimum is annihilated by these two saddle points merging toward each other. Therefore, in the regime $(1+\beta)d_{tot}/d_{DL} < 1$, the low density approximations falls short of predicting a globally stable state. It is possible that the system finds a stable ground state at some higher densities. (Ming: I'm not very clear here.) One can always choose interlayer spacing in a way such that the system is in the desired stable regime.

2.4 Dynamic conductance measurement

Since no current flows after the system reaches the equilibrium state, static measurements cannot reveal any information about the excitonic crossed Andreev tunneling process. To detect the tunneling process experimentally, we propose a dynamic measurement by applying a small amplitude AC voltage on top of the DC bias,

$$V_b(t) = V_{dc} + V_{ac}\cos\omega t. \tag{2.15}$$

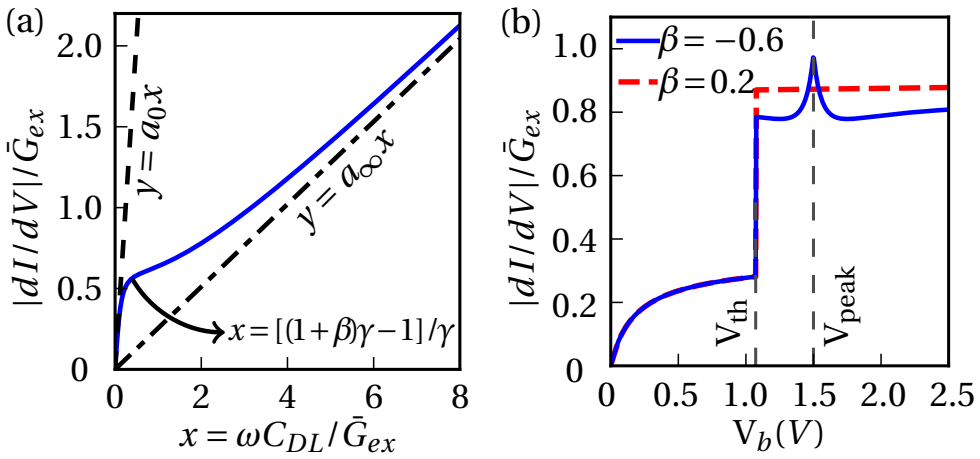

Figure 2.4: (Color online) Differential conductance as a function of (a) $x = \omega C_{DL}/\bar{G}_{ex}$ and (b) bias voltage V_b. The dashed line and the dash-dotted line in (a) shows the linear relation at low and high frequency limits respectively. The differential conductance starts to deviate from the low frequency linear behavior at the turning point where $x_0 = [(1+\beta)\gamma - 1]/\gamma$. The voltage dependence is plotted for $x = 1$ at two different values of β: blue solid line for $\beta = -0.6$ and red dashed line for $\beta = 0.2$. For $\beta < 0$, a peak emerges at voltage $V_{\rm peak} = -E^0_{ex}/\beta$ where n_S vanishes.

We solve for the response of n_S and n_{ex} to the AC bias by linearizing Eq. (2.13) and (2.9) assuming,

$$n_{ex}(t) = \bar{n}_{ex} + n^c_{ex}\cos\omega t + n^s_{ex}\sin\omega t \tag{2.16}$$

$$n_S(t) = \bar{n}_S \ + n^c_S\cos\omega t + n^s_S\sin\omega t, \tag{2.17}$$

where $\bar{n}_{ex}$ and $\bar{n}_S$ are the static components and n^s and n^c the magnitudes of the AC components.

The total current between the source and the drain is given by

$$I(t) = I_{ex}(t) + I_S(t) \tag{2.18}$$

where $I_{ex}(t) = Aedn_{ex}(t)/dt$ is the excitonic crossed Andreev tunneling current and $I_S(t) = Aedn_S(t)/dt$ the displacement current between the source and the top TMD layer. Both of these two currents have a zero average value and for $V_{dc} < V_{\rm th}$, I_{ex} is zero and only I_S contributes to the total current.

We present the results in terms of the differential conductance dI/dV which is a widely employed experimental probe. Fig. 2.4 shows the normalized amplitudes of the differential conductance $|dI/dV|/\bar{G}_{ex}$, where $\bar{G}_{ex}$ is the static component of G_{ex}. In the low frequency limit, electrons and holes have long enough time to tunnel to the TMD double layer so that the source and the drain capacitors are effectively "shorted". The system behaves as an effective capacitor $C^*_{DL} = a_0 C_{DL}$ which has a complex differential conductance with a phase of $\pi/2$ and an amplitude $|dI/dV|$ depending linearly on frequency ω, or equivalently $|dI/dV|/\bar{G}_{ex} = a_0 x$, shown as dashed line in Fig. 2.4(a). The

proportional constant is $a_0 = \{(\gamma-1)^2/[(1+\beta)\gamma - 1] + 1\}/\gamma$. When the exchange coupling is ignored, $a_0 = 1$ and one recovers $C^*_{DL} = C_{DL}$.

We observe that the response deviates from linear relation when the frequency reaches the turning point located roughly at $x_0 = [(1+\beta)\gamma - 1]/\gamma$. We propose that by measuring the frequency ω_0 of this turning point the tunneling conductance can be obtained as $\bar{G}_{ex} = \omega_0 C_{DL}/x_0$. In the high frequency limit, the tunneling channel is instead shorted by the source and the drain capacitors, the AC signal instead probes the total capacitance of the system, which is $(2/C_Q^{-1} + C_{geo}^{-1})^{-1} = C_{DL}/\gamma$. The differential conductance approaches the linear relation $a_\infty x$ asymptotically with $a_\infty = 1/\gamma$ (dash-dotted line in Fig. 2.4 a).

The voltage dependence of the differential conductance is shown in Fig. 2.4 b. The blue solid line shows the case for $\beta < 0$. A peak appears at $V_{\rm peak} = -E^0_{ex}/\beta$ where n_S becomes zero. This suggests a straightforward way to measure the exchange coupling strength g_X provided the size of the gap and the exciton binding energy are known. For $\beta > 0$ (red dashed line), the differential conductance increases slowly with increasing V_b.

2.5 Summary and discussion

We have developed a microscopic theory for the two-particle tunneling process which dominates the tunneling transport in the cases when the bias voltage is less than the energy gap of charged quasiparticle excitation and greater than the exciton chemical potential. The tunneling conductance is

calculated analytically using a second order perturbation theory and is proportional to the population of final exciton states which are assumed to be negligible for non-condensed sates. This process is not restricted by the spin and momentum selection rules as is the case for exciton radiative decay process and can be used to both populate and probe fluids of excitons while overcoming the shortcomings of optical measurement. In DC bias cases, the bias dependence of both the exciton density and the source density showed a threshold hold behavior and varies with the strength of exchange interaction. When a small signal AC bias is applied, the differential conductance is linearly dependent on frequency in the low and the high frequency limit and the frequency where it deviates from the linear trend in the low frequency can be used to determine the two-particle tunneling conductance. For negative exchange coupling strength, the differential conductance has a peak at voltage V_{peak} which directly measures the exchange coupling strength.

Chapter 3

Excitonic thermo-electric cooling device

3.1 Introduction

Since the discovery of the first thermoelectric phenomenon by Thomas Seebeck in 1822, people has been longing for high efficiency solid-state based devices for pumping or generation of heat that could surpass the conventional compression-based refrigerator [44]. Without relying on mechanical movements, solid-state based thermoelectric devices uses electrons and holes as heat carriers whose movement is controlled by electricity [30, 36, 45, 55]. Here, based on the coherent two-particle tunneling process, we propose an unusual thermoelectric cooling device in which excitons are the heat carriers [84].

In this chapter, I will first develop the theory for electrical injection based on this tunneling process in Sec. 3.2. The structure of the device is similar to the conventional two leg structure except a double quantum well is in place of the conductors. The section (Sec. 3.3) derive the transport coefficient for excitons without the presence of contacts. In the last section a Boltzmann equation is given which accounts for decay of excitons under the relaxation time approximation and the generation or absorption due to the two-particle tunneling from or to the contacts.

3.2 Coherent excitonic two-particle tunneling

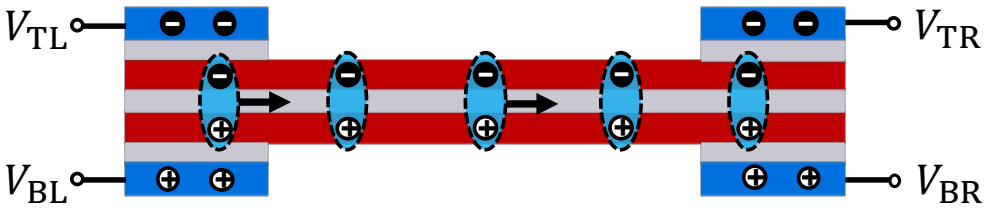

Figure 3.1: (Color online) Schematic illustration of the four-contact geometry. Separate contacts on made on both ends of the bilayer structure where heat is transport from one to another by excitons that follow between them. The direction of flow is controlled by the bias voltages V_{TL}, V_{BL}, V_{TR} and V_{BR}.

Consider a double quantum well (DQW) structure with electrical contacts made to the left and the right ends of each quatum well (QW) as shown in Fig. 3.1. We assume the top-left (TL) and top-right (TR) contacts are n-type while the bottom-left (BL) and bottom-right (BR) contacts are p-type. The DQW has a type-II band-alignment, with the lowest conduction band in the top QW and the higest valence band in the bottom QW, and forms an indirect bandgap. The low energy excitations in this sytem is then the spatially indirect excitons. Becasue excitons have energy below the indirect bandgap, we are able to use subgap bias voltage to inject excitons and in an ideal case supress the population of free carriers, i.e. free electrons in the top QW and free holes in the bottom QW, which increases exciton scattering rate and lowers the cooling efficiency. With proper bias scheme, excitons are generated on the one end of the structure, flow to the other end where they are ionized into electrons and holes in the contacts. Because of the spatial separation, we

assume that the lifetime of excitons can be made long compared to the decay rate and to the time scale needed for excitons to flow across the length in the transport direction.

In this section, we develop a theory describing the exciton injection process based on the coherent two-particle tunneling mechanism. Assuming the bias voltages are small such that local equilibrium approximation is valid. We assume the contact areas are small such that the area under them can be considered to be in a local equilibrium also. The theory we describe below works for contact areas in both ends.

The total Hamiltonian in the contact area can be written as

$$\hat{\mathcal{H}} = \hat{\mathcal{H}}_T + \hat{\mathcal{H}}_B + \hat{\mathcal{H}}_{DQW} + \hat{\mathcal{H}}_t. \tag{3.1}$$

The first two terms represent the non-interacting Hamiltonian of the top and the bottom contacts which we assume to be doped semicondcutors,

$$\hat{\mathcal{H}}_\alpha = \sum_{\bar{\boldsymbol{p}}} \epsilon^\alpha_{\bar{\boldsymbol{p}}}\, \hat{a}^\dagger_{\bar{\boldsymbol{p}},\alpha} \hat{a}_{\bar{\boldsymbol{p}},\alpha}, \tag{3.2}$$

where $\alpha = T, B$ and $\bar{\boldsymbol{p}} = (\lambda, s, \boldsymbol{p})$ is a compound index of band index λ, spin s and momentum $\boldsymbol{p}$. $\hat{a}^\dagger$ and $\hat{a}$ are creation and annihilation operators for electrons in the contacts. $\epsilon^\alpha_{\bar{\boldsymbol{p}}}$ is the energy dispersion which we assume to be quadratic. The next term is the interacting hamiltonian of the DQW,

$$\hat{\mathcal{H}}_{DQW} = \sum_{\boldsymbol{k},\beta} \epsilon^\beta_{\boldsymbol{k}} \hat{c}^\dagger_{\boldsymbol{k},\beta} \hat{c}_{\boldsymbol{k},\beta} + \frac{1}{2A} \sum_{\beta,\beta'} \sum_{\boldsymbol{q},\boldsymbol{k},\boldsymbol{k}'} V_{\beta\beta'}(\boldsymbol{q}) \hat{c}^\dagger_{\boldsymbol{k}+\boldsymbol{q},\beta} \hat{c}^\dagger_{\boldsymbol{k}'-\boldsymbol{q},\beta'} \hat{c}_{\boldsymbol{k}',\beta'} \hat{c}_{\boldsymbol{k},\beta} \tag{3.3}$$

where $\beta = c, v$ indicate the lowest conduction band and the highest valence band respectively. $\hat{c}^\dagger$ and $\hat{c}$ are creation and annihilation operators for electrons in the DQW. $V_{\beta\beta'}(\boldsymbol{q}) = 2\pi e^2 e^{-|\boldsymbol{q}|d_{\beta\beta'}}/(\epsilon|\boldsymbol{q}|)$ is the Coulomb interaction potential, where the diagonal components $d_{\beta\beta}$ are zero and the offdiagonal components $d_{cv} = d_{vc} \equiv d_0$ denote the inter-well spacing of the DQW. ϵ is the dielectric constant of the insulating barrier between them. Note that we have retained only one band in each QW because the other bands don't contribute to the tunneling process.

Electron tunneling between QWs is described by the Hamiltonian

$$\hat{\mathcal{H}}_t = \sum_{\boldsymbol{k},\bar{\boldsymbol{p}}} t^T_{\boldsymbol{k}\bar{\boldsymbol{p}}} \hat{c}^\dagger_{\boldsymbol{k},c} \hat{a}_{\bar{\boldsymbol{p}},T} + t^B_{\boldsymbol{k}\bar{\boldsymbol{p}}} \hat{c}^\dagger_{\boldsymbol{k},v} \hat{a}_{\bar{\boldsymbol{p}},B} + h.c. \tag{3.4}$$

where $t^{T(B)}_{\boldsymbol{k}\bar{\boldsymbol{p}}}$ are the tunneling matrix elements. We have neglected tunneling between the QWs because it is a channel for electron-hole recombination which is assumed to be negligible in our model.

Fig. 3.2b shows the schematic band diagram of the contact region under local equilirbrium approximation. When no bias is applied, we assume the band structure is symmetric with respect to the zero of energy, which is chosen to be the center of the indirect bandgap E_g. When a subgap bias voltage $E_g > eV_{\mathrm{BT}} > 0$, where $V_{\mathrm{BT}} \equiv V_{\mathrm{B}} - V_{\mathrm{T}}$ and $e > 0$ is the unit of charge, is applied, normal tunneling between the top contact and the QW1 is prohibited by energy conservation. Direct tunneling of electrons between the top and the bottom contact is also highly suppressed because it must overcome three tunneling barriers. One can enable normal tunneling by increasing the bias

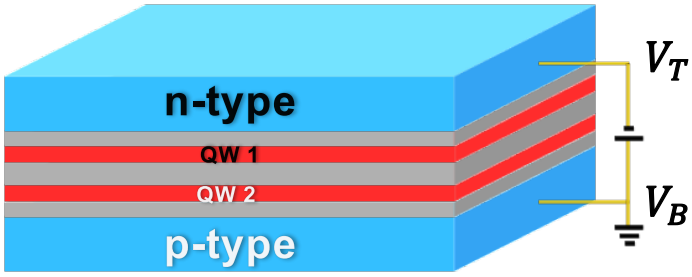

(a)

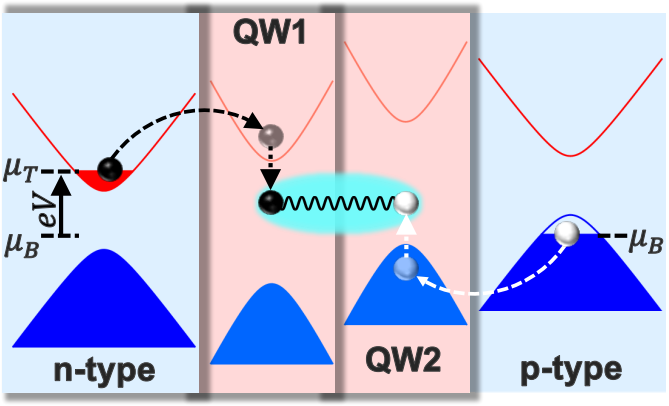

(b)

Figure 3.2: (a). Local structure at the contact region. (b) Bandstructure of the contact region under the local equilibrium approximation. From left to right are the top contact, QW 1, QW 2 and the bottom contact. The figure also illustrates the bias scheme which allows creation of excitons at the local area.

voltage all the way to above the indirect band gap $eV_{\rm BT} > E_g$. In this case, electrons with high enough energy could tunnel directly from the contacts to the QWs and conduction-to-conduction tunneling between QWs becomes possible. Consequently, electrons can tunnel from the top to the bottom contact via three consecutive first order tunneling processes.

The exciton generation process that we are interested in lies in the bias regime $E_g > eV_{\rm BT} > \mu_{ex}$ where electrons can tunnel via the many body states, i.e. spatially indirect excitons, which have energies $E_{\rm ex}(\boldsymbol{Q})$ lower than the indirect band gap E_g. It is a second order process involving two tunneling steps (as illustrated in Fig. 3.2b) which effectively transfers one electron from the top to the bottom contact and create one exciton. This is the dominant tunneling process in the subgap regime because normal tunneling via single particle states are of higher orders in tunneling amplitudes.

The coherent two-particle tunneling rate can be obtained using Fermi's golden rule to the second order in $\hat{\mathcal{H}}_t$,

$$\left(\frac{\partial n_{\rm ex}(\boldsymbol{Q})}{\partial t}\right)_{\rm inj} = \frac{2\pi}{\hbar}\sum_{p_T,p_B}\left|M(\boldsymbol{Q};\boldsymbol{p}_T,\boldsymbol{p}_B)\right|^2\left[n_{\rm ex}(\boldsymbol{Q})+1\right] \times\left[f^T_{\boldsymbol{p}_T}-f^B_{\boldsymbol{p}_B}\right]\delta\left(\epsilon^T_{\boldsymbol{p}_T}-\epsilon^B_{\boldsymbol{p}_B}-E_{\rm ex}(\boldsymbol{Q})\right) \tag{3.5}$$

where the partial derivative means the change of exciton density due to this electrical injection process. The matrix element is defined as,

$$M(\boldsymbol{Q};\boldsymbol{p}_T,\boldsymbol{p}_B) = \sum_{\boldsymbol{k}}\phi_{\boldsymbol{k}}t^T_{\boldsymbol{k}+\boldsymbol{Q}/2,\boldsymbol{p}_T}t^{B*}_{\boldsymbol{k}-\boldsymbol{Q}/2,\boldsymbol{p}_B}\left\{\frac{1}{\epsilon^c_{\boldsymbol{k}+\boldsymbol{Q}/2}-\epsilon^T_{\boldsymbol{p}_T}}+\frac{1}{\epsilon^B_{\boldsymbol{p}_B}-\epsilon^v_{\boldsymbol{k}-\boldsymbol{Q}/2}}\right\}. \tag{3.6}$$

where $\phi_{\boldsymbol{k}}$ is the momentum space wavefunction for internal motion of excitons. The factor $n_{\rm ex}(\boldsymbol{Q})+1$ appering on the right-hand side of Eq. (3.5) is due to the bosonic final state stimulation. The crucial difference between the coherent tunnling and the incoherent injection is the dependence on the Fermi distribution factors. In a incoherent injection setup, the generation rate would be proportional to the product of the occupation numbers of excited electrons and holes in the DQW.

For simplicity, we make the crude approximation that the matrix element $M(\boldsymbol{Q};\boldsymbol{p}_{_T},\boldsymbol{p}_{_B})$ is independent of the exciton momentum $\boldsymbol{Q}$ which is true in many system where the tunneling process is momentum non-conserving and independent. We can thus arrive at the approximate relation

$$\left(\frac{\partial n_{\rm ex}(\boldsymbol{Q})}{\partial t}\right)_{\rm inj} \approx g_{\rm ex}\cdot\big(n_{\rm ex}(\boldsymbol{Q})+1\big)(eV_{\rm BT}-E_{\rm ex}(\boldsymbol{Q})) \tag{3.7}$$

This relation defines the generation and decay terms for the Boltzmann equation that we are going to solve for the four-contact geometry in Sec. 3.4

3.3 Thermoelectric transport coefficients

In this section, we calculate the exciton thermoelectric transport coefficients. We employ the relaxation time approximation [4]

$$\frac{\partial n^{(0)}_{\rm ex}(\boldsymbol{Q},x)}{\hbar\partial\boldsymbol{Q}}\cdot\boldsymbol{\nabla}\mu_{\rm ex}+\frac{\partial n^{(0)}_{\rm ex}(\boldsymbol{Q},x)}{\partial T}\boldsymbol{v}_{\boldsymbol{Q}}\cdot\boldsymbol{\nabla}T=\frac{n^{(1)}_{\rm ex}(\boldsymbol{Q},x)}{\tau_{\rm ex}} \tag{3.8}$$

where T is temperature and $\mu_{\rm ex}$ the exciton chemical potential. The exciton group velocity is given by $\boldsymbol{v}_{\boldsymbol{Q}}\equiv\partial E_{\rm ex}(\boldsymbol{Q})/\hbar\partial\boldsymbol{Q}$. Here we assumed a homoge-

neous exciton decay rate $\tau_{\rm ex}$ to account for the radiative electron-hole recombination process. Note that expressing the force in terms of chemical gradient has the advangtage of being independent of the particle's charge.

The electric current can then be calculated as

$$\boldsymbol{j} = e\tau_{\rm ex} \sum_{\boldsymbol{Q}} \frac{\partial n_{\rm ex}^{(0)}(\boldsymbol{Q}, x)}{\partial E_{\rm ex}(\boldsymbol{Q})} \boldsymbol{v}_{\boldsymbol{Q}} \boldsymbol{v}_{\boldsymbol{Q}} \cdot \left[\boldsymbol{\nabla} \mu + \frac{E_{\rm ex}(\boldsymbol{Q}) - \mu_{\rm ex}}{T} \boldsymbol{\nabla} T \right] \tag{3.9}$$

and the thermal current is given by

$$\boldsymbol{j}_{\rm th} = \tau_{\rm ex} \sum_{\boldsymbol{Q}} \frac{\partial n_{\rm ex}^{(0)}(\boldsymbol{Q}, x)}{\partial E_{\rm ex}(\boldsymbol{Q})} \big(E_{\rm ex}(\boldsymbol{Q}) - \mu_{\rm ex}\big) \boldsymbol{v}_{\boldsymbol{Q}} \boldsymbol{v}_{\boldsymbol{Q}} \cdot \left[\boldsymbol{\nabla} \mu_{\rm ex} + \frac{E_{\rm ex}(\boldsymbol{Q}) - \mu_{\rm ex}}{T} \boldsymbol{\nabla} T \right] \tag{3.10}$$

We are interested in the longitudinal components of the transport coefficients. Assuming the temperature and the chemical potential gradients are along the x direction, so $\boldsymbol{j} = j\boldsymbol{e}_x$ and $\boldsymbol{j}_{\rm th} = j_{\rm th}\boldsymbol{e}_x$. We define the transport coefficient by writting Eq. (3.9)-(3.10) as:

$$\begin{aligned} j &= \mathcal{L}_{11} \partial_x \mu_{\rm ex} + \mathcal{L}_{12} \partial_x T \\ j_{\rm th} &= \mathcal{L}_{21} \partial_x \mu_{\rm ex} + \mathcal{L}_{22} \partial_x T. \end{aligned} \tag{3.11}$$

Thermopower (also called Seebeck coefficient) $\alpha_{\rm ex}$ is defined in the situation when there is no electric current $j = 0$ due to the cancellation between the electric field E_x coming from the charge accumulation and the temperature gradient [4, 55]. In this case, we have

$$\alpha_{\rm ex} = \frac{E_x}{\nabla T} = \frac{1}{e} \frac{\nabla \mu}{\nabla T} \tag{3.12}$$

Using Eq. (3.9) and assuming $E_{\rm ex}(\boldsymbol{Q}) = E^0_{\rm ex} + \hbar^2\boldsymbol{Q}^2/2m_{\rm ex}$ and $\mu_{\rm ex} < 0$ for excitons, we obtain

$$\alpha_{\rm ex} = -\frac{\mathcal{L}_{11}}{e\mathcal{L}_{12}} = -\frac{2k\mathrm{Li}_2(\exp(\mu_{\rm ex}/kT))}{e\mathrm{Ln}(1-\exp(\mu_{\rm ex}/kT))} - \frac{\mu_{\rm ex}}{eT} \tag{3.13}$$

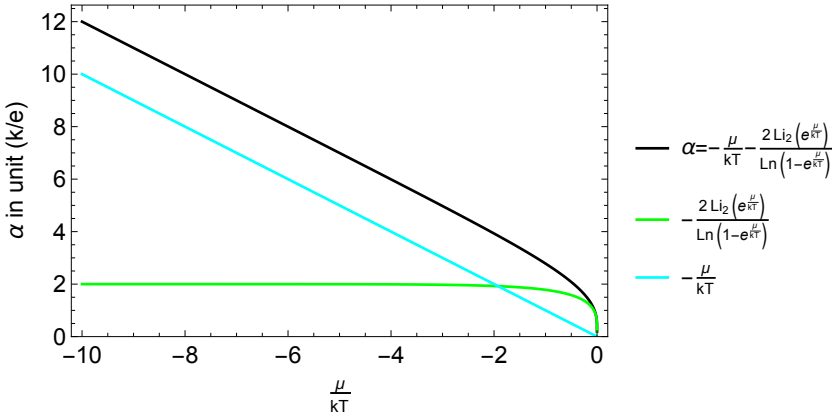

Figure 3.3: Seebeck coefficient as a function of μ/kT

The thermal conductivity is defined as the coefficient of the temperature gradient in the thermal current when there is no electric current flow

$$\kappa_{\rm ex} = \mathcal{L}_{22} - \frac{\mathcal{L}_{12}}{\mathcal{L}_{11}}\mathcal{L}_{21} \tag{3.14}$$

and the electric conductivity is

$$\sigma_{\rm ex} = e\mathcal{L}_{11} = \frac{2e^2\tau_{\rm ex}}{m_{\rm ex}} \sum_{\boldsymbol{Q}} \frac{\partial n^{(0)}_{\rm ex}(\boldsymbol{Q}, x)}{\partial E_{\rm ex}(\boldsymbol{Q})} E(\boldsymbol{Q}) \cos^2\theta_{\boldsymbol{Q}} \tag{3.15}$$

The Lorenz number is given by

$$\begin{aligned} L_{\rm ex} &= \frac{\kappa_{\rm ex}}{\sigma_{\rm ex}T} = \frac{\mathcal{L}_{22}\mathcal{L}_{11} - \mathcal{L}_{12}\mathcal{L}_{21}}{e\mathcal{L}^2_{11}} \\ &= \left(\frac{k}{e}\right)^2 \left\{ \frac{6\mathrm{Li}_3(\exp(\mu_{\rm ex}/kT)}{-\mathrm{Ln}(1-\exp(\mu_{\rm ex}/kT)} - \left[\frac{2\mathrm{Li}_2(\exp(\mu_{\rm ex}/kT)}{-\mathrm{Ln}(1-\exp(\mu_{\rm ex}/kT)}\right]^2 \right\} \end{aligned} \tag{3.16}$$

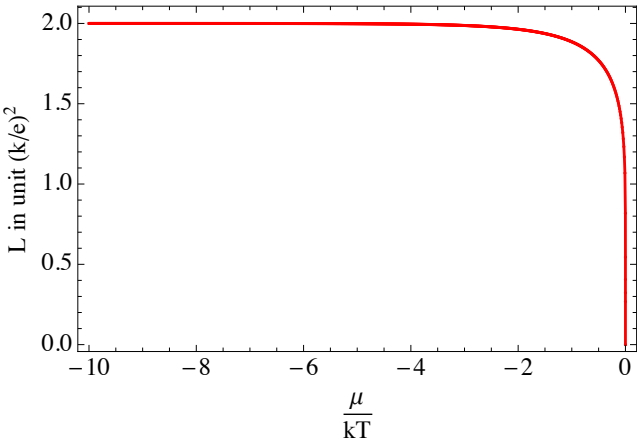

(a)

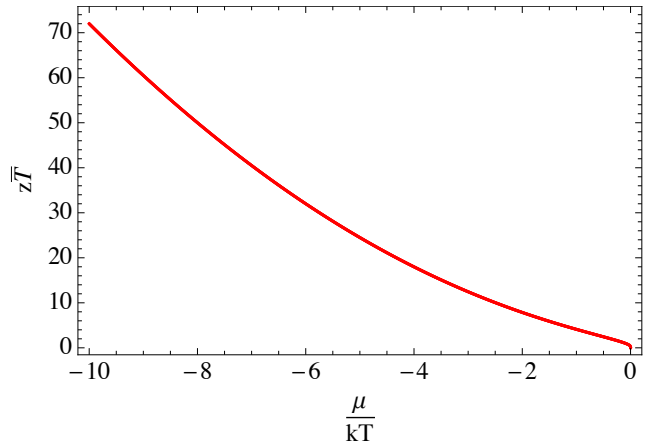

(b)

Figure 3.4: (a). Lorenz number L_{ex} as a function of μ_{ex}/kT. (b). Figure of merit $z\bar{T}_{\text{ex}}$ as a function of μ_{ex}/kT.

Finally, we arrive at the result for the figure of merit [55]

$$z\bar{T}_{\text{ex}} = \frac{\alpha_{\text{ex}}^2 \sigma_{\text{ex}} \bar{T}}{\kappa_{\text{ex}}} = \frac{\alpha_{\text{ex}}^2}{L_{\text{ex}}} \tag{3.17}$$

We estimate the thermopower for some typical experimental parameters

$$\kappa_{\rm ex} = \sigma_{\rm ex} T L_{\rm ex} = \frac{e^2 \tau_{\rm ex} n_{\rm ex}}{m_{\rm ex}} T \left(\frac{k}{e}\right)^2 = \frac{n_{\rm ex}\hbar^2}{m_{\rm ex}} \frac{kT}{\hbar/\tau_{\rm ex}} \frac{k}{\hbar} \tag{3.18}$$

For bulk system, we replace $n_{\rm ex}$ by $n^{3D} = n a_B^{-3}$, so our results have the dimension for bulk thermopower and n is dimensionless parameter. Then we have $n^{3D}\hbar^2/m = n{\rm Ry}/a_B$. Assume following order of estimation: $\hbar/\tau \approx 25meV \approx kT$. Given $\hbar = 1.05 \times 10^{-34} J \cdot s$ and $k = 1.38 \times 10^{-23} J/K$, one can estimate roughly

$$\kappa_{\rm ex} \approx \frac{n \times 10^{-18} J}{10^{-10} m} \times 1 \times \frac{10^{-23} J/K}{10^{-34} J \cdot s} \approx n \times 10^3 \frac{W}{m \cdot K} \tag{3.19}$$

For comparison, the phonon contribution to thermalpowr in bulk WSe_2 is measured to be

$$\kappa_{\rm ex}|_{\rm WSe_2} = 1 \frac{W}{m \cdot K} \tag{3.20}$$

3.4 Four-contact geometry

In this section we consider the presence of the four-contacts which generates and absorbs excitons. We employ the Boltzmann equation and relaxation time approximation to calculate the transport coefficient. Assuming that within the contact area all the quantities are uniform, we can approximate the left and the right contact regions by points at $x = 0$ and $x = L$ respectively.

Using the result from Eq. (3.7) for both the left and the right contact region,

$$\left(\frac{\partial n_{\mathrm{ex}}(\boldsymbol{Q},x)}{\partial t}\right)_{\mathrm{inj},x=0} \approx g_{\mathrm{ex}} \cdot \big(n_{\mathrm{ex}}(\boldsymbol{Q},0)+1\big)\big[e(V_{\mathrm{LB}}-V_{\mathrm{LT}})-E_{\mathrm{ex}}(\boldsymbol{Q},0)\big] \tag{3.21}$$

$$\left(\frac{\partial n_{\mathrm{ex}}(\boldsymbol{Q},x)}{\partial t}\right)_{\mathrm{inj},x=L} \approx g_{\mathrm{ex}} \cdot \big(n_{\mathrm{ex}}(\boldsymbol{Q},L)+1\big)\big[e(V_{\mathrm{RB}}-V_{\mathrm{RT}})-E_{\mathrm{ex}}(\boldsymbol{Q},L)\big] \tag{3.22}$$

Including the above generation and decay terms into the Boltzmann equations, we obtain

$$\begin{aligned}&\frac{\partial n_{\mathrm{ex}}^{(0)}(\boldsymbol{Q},x)}{\partial t}+\frac{\partial n_{\mathrm{ex}}^{(0)}(\boldsymbol{Q},x)}{\hbar\partial \boldsymbol{Q}}\cdot\boldsymbol{\nabla}\mu_{\mathrm{ex}}+\frac{\partial n_{\mathrm{ex}}^{(0)}(\boldsymbol{Q},x)}{\partial T}\boldsymbol{v}_{\boldsymbol{Q}}\cdot\boldsymbol{\nabla}T\\ &=\frac{n_{\mathrm{ex}}^{(1)}(\boldsymbol{Q},x)}{\tau_{\mathrm{ex}}}+\left(\frac{\partial n_{\mathrm{ex}}(\boldsymbol{Q},x)}{\partial t}\right)_{\mathrm{inj},x=0}+\left(\frac{\partial n_{\mathrm{ex}}(\boldsymbol{Q},x)}{\partial t}\right)_{\mathrm{inj},x=L}\end{aligned} \tag{3.23}$$

This could be solved for different choices of the bias voltages V_{LT}, V_{LB}, V_{RT} and V_{RB}. Here we intends to present how we think this unusual thermoelectric device works and layout the theoretical formalism that is going to be used for quantitative analysis. The numerical result will be presented in a future publication based on the theory outlined in this chapter.

Chapter 4

Polariton supercurrent generation in unipolar electro-optic devices

4.1 Introduction

This work is motivated by remarkable progress over the past decade in realizing and exploring the physics of dynamical steady states of coupled light and matter in which two-dimensional exciton-polaritons, bosonic states that are coherent mixtures of vertical cavity photons and quantum-well excitons, condense into states with macroscopic coherence [5, 19, 20, 26, 48, 53, 69]. The achievement of exciton-polariton condensation can be viewed as an end point of the long quest for exciton condensation in semiconductors [10, 52] containing steady state populations of conduction band electrons and valence band holes. From this point of view, the role of the resonant coupling to vertical cavity photons, which turns excitons into exciton-polaritons, is to provide the bosonic particles with sufficient phase stiffness via the small polariton mass that is sufficient to combat disorder that would otherwise localize the excitons. In typical systems that steady-state polariton population is provided by optically exciting a population of non-resonant excitons that can be scattered into the condensate at a rate that balances the rate at which polariton population is lost by cavity-photon leakage. For many purposes the polariton system

environment can be approximated as a thermal reservoir. The polariton condensate can also be supported electrically by applying a bias voltage across a bipolar system so that the current is carried through the system by injecting conduction-band electrons at an n-contact and removing valence-band holes at a p-contact [8, 9].

In this article we describe a different mechanism for electrical manipulation of exciton-polariton condensates that can act even in unipolar systems. It is based on the properties of electronic quasiparticles in quantum wells or two-dimensional materials when they are dressed by interactions with the coherent exciton field of an exciton condensate, or the coherent exciton and photon fields of a polariton condensate, and relies on approximate conservation of the sum of the total photon and exciton numbers. Because it generates excitons or polaritons where the particle current exits the coherent cavity region and absorbs them when it enters, it does not yield a global exciton or exciton-polariton generation rate and thus cannot on its own support a finite bosonic particle population. It can however generate a supercurrent in the exciton or polariton condensate that flows between source and drain regions.

Our article is organized as follows. In Section II we explain the basic mechanism, which applies to both exciton and exciton-polariton condensate cases. Throughout this article we focus exclusively on the exciton-polariton case because it can be reliably realized experimentally. The basic idea is that when electronic quasiparticles are dressed by their interaction with an exciton-polariton condensate, they do not separately conserve conduction and

valence band currents. Conservation is recovered by compensating boson generation and absorption contributions to the condensate equation of motion which drives the condensate into a state that carries a super-current. This effect is partly analogous to supercurrent generation at normal-superdonducting interfaces, and to spin-transfer torques in ferromagnets, but has some surprising wrinkles. In particular the direction of the exciton-polariton supercurrent is opposite to the direction of charged particle flow. The transfer process between the quasiparticles and the condensate in general leads to source terms for different components of the exciton-polariton condensate, in a ratio that depends on the strength of the coupling of the quasiparticles to that component of the condensate. (In practice the quasiparticle-condensate transfer process mainly produces a source term for the exciton portion of the condensate.) In Section III we explain how separate transfer processes, proportional to Rabi coupling strengths, rearrange the composition of the current on a longer length scale so that it is ultimately carried by the lower-polariton condensate. In Section IV we examine the possibility of identifying these transfer effects experimentally by measuring the finite transverse momentum of the lower-polariton condensate when it carries a supercurrent. Finally in Section V we summarize our results, present conclusions, and speculate on possible applications.

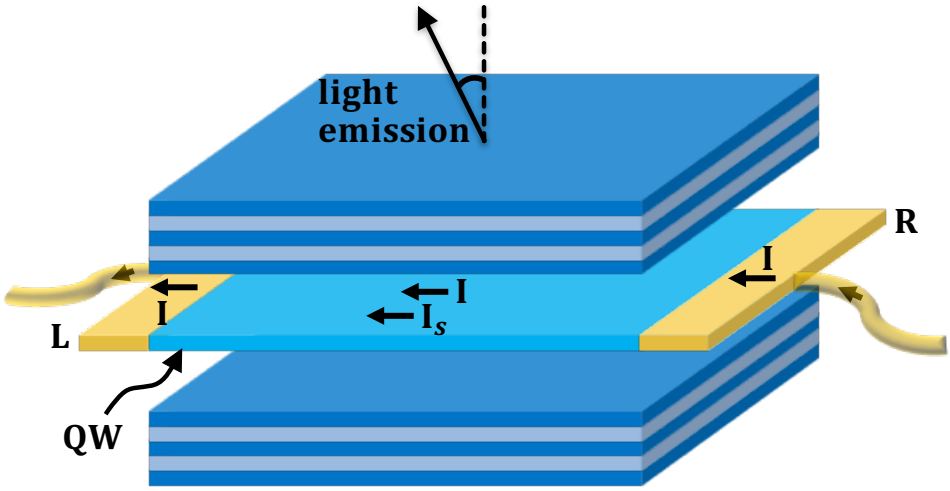

Figure 4.1: (Color online) Schematic representation of the planar semiconductor microcavity with contacts made to the quantum well.

4.2 Electrically driven exciton supercurrent

We illustrate the quasiparticle-condensate transfer effect by considering a planar semiconductor microcavity with electrical contact established to an embedded quantum well, as illustrated schematically in Fig. 4.1. For definiteness we assume that the contacts are n-type and that the quantum well is intrinsic, so that the electrical system is a lateral n-i-n homojunction. As we explain below, this geometry does not[1] support steady-state net electrically-controlled exciton or polariton generation. We therefore assume that a non-resonant optical pump is also present to maintain a finite steady-state polariton population in the cavity region. We are interested in the regime in which the pumping power exceeds the threshold for polariton condensate formation, and

a bias voltage is applied between the electrical contacts.

The influence of electrical transport on the polariton condensate can be understood in a two-step model. First, electric charge is injected from the left (L) contact, drained to the right (R) contact and transported through the cavity region by fermionic quasiparticles that carry an electrical charge and are dressed by the condensate. During this process, a neutral exciton supercurrent is induced in response to the charge current via a mechanism explained below. Second, the exciton supercurrent is converted to a lower polariton supercurrent. During this latter process, part of the exciton condensate momentum is transferred to the photonic component. This two step model is justified when the exciton-photon conversion length scale is much longer than the length scale over which the exciton supercurrent is generated.

We describe both the quantum well and the contacts with a two-band semiconductor model. The contacts, which are located outside of the cavity, are not dressed by the photon field, but the bare conduction and valence band states of the quantum well in the cavity region are coupled by both the coherent photon and the coherent exciton field. For the illustrative calculations we perform below, we assume that the coherence amplitude rises steeply at the n-i interface. The mean field Hamiltonian in the coherent region in the bare conduction-valence basis is

[1] All-electrical devices are also possible but require both n and p contacts. See for example Ming Xie and A.H. MacDonald, arXiv:1708. nnnn (in preparation). The $n-i-n$ geometry provides the simplest illustration of our quasiparticle-condensate transfer effect.

$$H = \begin{pmatrix} H_0 & g\psi(\mathbf{r}) + \Delta(\mathbf{r}) \\ g\psi(\mathbf{r}) + \Delta(\mathbf{r}) & -H_0 \end{pmatrix} \tag{4.1}$$

where $H_0 = -\hbar^2\nabla^2/2m + \delta/2$ and ∇ is the 2D gradient operator. For simplicity, we have taken the effective masses m of the two bands to be identical and isotropic. We further simplify the problem by assuming that the system is translationally invariant in the transverse (y) direction and neglecting electrostatic band bending effects.

The Hamiltonian (4.1) is written in a rotating-wave frame in which the condensate energy is effectively absorbed into the energy of electrons, so that the actual bandgap E_g is replaced by a reduced gap $\delta \equiv E_g - \hbar\omega$ where $\hbar\omega$ is the chemical potential of the condensate. For typical polariton condensates δ is of the same order [18, 47, 87] as the two-dimensional exciton binding energy. In the two band model rotating and fixed (f) representation wavefunctions are related by

$$\Psi(\mathbf{r}, t) = \hat{U}^{-1}(t)\Psi_{\mathrm{f}}(\mathbf{r}, t) \tag{4.2}$$

where $\hat{U}(t) = \exp(-\frac{i}{2}\omega t\sigma_z)$ and σ_z is the band Pauli-matrix. Here $\Psi(\mathbf{r}, t) = (u(\mathbf{r}, t), v(\mathbf{r}, t))^T$ is a two-component vector whose components are the conduction and valence components of the quasiparticle wavefunction.

The two terms in the off-diagonal component of the Hamiltonian originate from electron-photon coupling and from Coulomb interactions [18, 47, 87] respectively, and are time-independent in the rotating representation. In the

electron-photon coupling term g is the electric dipole coupling constant and $\psi = \langle \hat{a} \rangle$ is the coherent photon field, *i.e.* the expectation value of the photon annihilation operator $\hat{a}$ in the coherent photon state. Δ is a mean field describing coherence induced by interband exchange interactions, which are also the origin of the attractive force that binds electrons and holes in an isolated exciton. Both $g\psi$ and Δ are chosen to be real and constant across the cavity region($0 < x < L$). In the left ($x < 0$) and the right ($x > L$) contact $g\psi = 0$ and $\Delta = 0$. The matter-photon transfer effect we describe below occurs because of spatial variation in the inter-band coupling terms in (4.1).

In the rotating representation the quasiparticle Hamiltonian is time independent and its wavefunction $\Psi(\mathbf{r}, t)$ satisfies a time-independent Schrödinger equation. The quasiparticle-condensate transfer effect is most simply illustrated by assuming ballistic transport. We therefore postpone a discussion of scattering effects to the discussion section. Due to translational symmetry in the y direction, the transverse momentum k_y is a good quantum number. For each k_y the x-dependent factor in the wavefunction satisfies a one-dimensional Schrödinger equation with $H_0 \to H_0^{\rm eff}(k_y) = -\hbar^2\nabla_x^2/2m + \delta_{k_y}^{\rm eff}/2$, where we defined an effective bandgap $\delta_{k_y}^{\rm eff} = \delta + \hbar^2 k_y^2/m$. In the cavity region, the bulk quasiparticle energies are $E_{\mathbf{k}}^{\pm} = \pm\sqrt{\xi_{\mathbf{k}}^2 + (g\psi + \Delta)^2}$, where $\xi_{\mathbf{k}} = \hbar^2 k_x^2/2m + \delta_{k_y}^{\rm eff}/2$, and the quasiparticle wavefunction has mixed conduction and valence band character. We define a k_y-dependent quasiparticle bandgap $\delta'_{k_y} \equiv \sqrt{(\delta_{k_y}^{\rm eff})^2 + 4(g\psi + \Delta)^2}$. Fig. 4.2 plots the transmission probability for a $k_y = 0$ electron incident (I) from the left contact as a function of

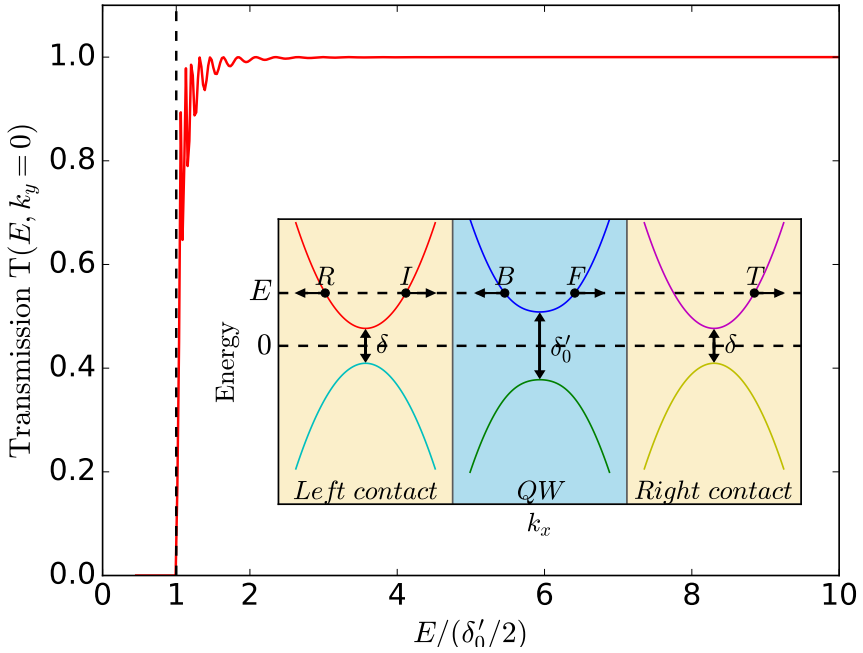

Figure 4.2: (color online) Energy dependence of the transmission probability for normal incidence $k_y = 0$. The transition probability decays exponentially with channel length for $|E| < \delta_0'/2$, where δ_0' is the renormalized quasiparticle gap. Inset: Model energy dispersions in different regions for $\delta = 10$meV and $g\psi + \Delta = 10$meV.

energy E. For $E > \delta_0'/2$ propagating modes are present in the cavity region and the transmission probabilities between source and drain contacts are large. Because the channel length exceeds microscopic length scales, the transmission probability jumps sharply from near 0 to near 1 at the band edge. (The oscillatory behavior in Fig. 4.2 is a consequence of multiple reflection between source/bulk and bulk/drain interfaces.)

Because the condensate is charge neutral, electric current in the QW

is carried by quasiparticle excitations only. For energy $E > \delta'_{k_y}/2$ the cavity region has two conduction-band dominated propagating Schrödinger equation solutions with real wavevectors $\pm k_x^+$, and two valence-band dominated evanescent Schrödinger equation solutions with imaginary wavevectors $\pm k_x^-$. Here $k_x^\pm = 2m\sqrt{-\delta_{k_y}^{\rm eff}/2 \pm (E^2 - (g\psi + \Delta)^2)^{1/2}}/\hbar^2$. We solve the elastic scattering problem by matching the wavefunction and its derivative at the two interfaces and conserving transverse momentum [11,67]. Quasiparticle flow is characterized by the counter flow of its conduction and valence component. From the mean field equation, we obtain the following coupled continuity relations

$$\frac{\partial |u|^2}{\partial t} + \nabla_x j_c = \frac{2(g\psi + \Delta)}{\hbar} {\rm Im}\{u^* v\} \tag{4.3}$$

$$\frac{\partial |v|^2}{\partial t} + \nabla_x j_v = -\frac{2(g\psi + \Delta)}{\hbar} {\rm Im}\{u^* v\} \tag{4.4}$$

where $j_c = \hbar {\rm Im}\{u^* \nabla_x u\}/m$ and $j_v = -\hbar {\rm Im}\{v^* \nabla_x v\}/m$. (We have suppressed the (E, k_y, x) dependence of the wavefunctions and the probability current densities for notational convenience.) These relations lead directly to the conservation law of particle current $\partial\rho/\partial t + \nabla_x j = 0$, where $\rho = |u|^2 + |v|^2$ is the particle density and $j = j_c + j_v$ the corresponding probability current density. In a steady state, j is spatially constant as shown in Fig. 4.3(a).

The key observation from Fig. 4.3 is that because the quasiparticles in the coherent cavity region are coupled to the condensate, the individual currents j_c and j_v are not separately conserved. In analogy with the spin density in a spin-$\frac{1}{2}$ system, we can define a difference density $\rho_- \equiv |u|^2 - |v|^2$ which can be interpreted as the exciton probability distribution. The associ-

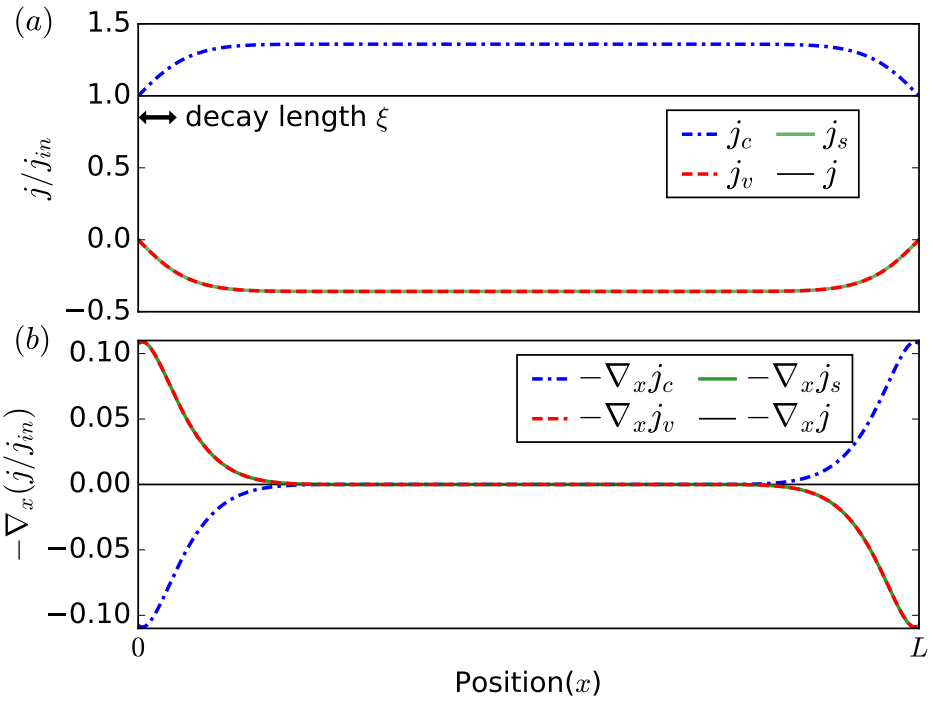

Figure 4.3: (color online) Spatial dependence of (a) normalized conduction and valence band partial probability currents and (b) divergence of the probability currents inside the QW for normal incidence $k_y = 0$ with $E = 0.55\delta_0'$. $j_{\rm in}$ is the current incident from the left contact. For the chosen parameters, the decay length $\xi \approx 1.8$ nm is much smaller than the channel length L.

ated continuity relation has the form $\partial\rho_-/\partial t + \nabla_x j_- = 4(\tilde{g}\psi + \Delta)\mathrm{Im}\{u^* v\}/\hbar$, where $j_- \equiv j_{\rm c} - j_{\rm v}$ is the corresponding electron-hole (or counter-flow) current. The source(or drain) term on the right-hand side is proportional to the coherence amplitude and large in the transition region between contact and cavity (Fig. 4.3(b)). Since the microscopic model neglects processes, other than coupling to the cavity photon, which violate separate particle-number conservation, a compensating source or drain term appears in the equation of motion for

the condensate and restores the symmetry. (See the explicit discussion in the supplementary material.) These conservation terms are precisely analogous to those that produce Cooper-pair source and drain terms when current flows across a normal-metal/superconductor [3] interface, and to the spin-transfer torque [76] contribution to the equation of motion for a magnetic condensate in inhomogeneous magnetic systems. In both of these cases the conservation law is restored by the action of the quasiparticles on the collective degrees of freedom of the condensate. In our case, because the quasiparticles interact much more strongly [87] with the excitonic part of the condensate than with the cavity photons, the quasiparticles act primarily as a source for the excitonic part of the condensate. It follows that $\nabla_x j_{\mathrm{s}} = -2(\tilde{g}\psi + \Delta)\mathrm{Im}[u^* v]/\hbar$. Including this superfluid component, the conservation is recovered for the total electron-hole probability current $j_{\text{e-h}} = j_- + 2j_s$, where the factor 2 appears because we define j_s as the pair probability current. Fig. 4.3(b) shows the divergence of the probability currents along the transport direction which represents the rate of transfer between the quasiparticles and the condensate.

As indicated in Fig. 4.3, the length scale over which the quasiparticle-condensate transfer occurs is short. From our calculation we can associate this length with the decay length of the evanescent valence-band dominated Schrödinger equation solutions at conduction band energies. Away from the interfaces, only propagating modes survive so j_s saturates at its asymptotic value j_s^{sat}. An analytical result can be obtained for j_s^{sat} as follows. Consider two cross sections one deep in the left contact $x = -\infty$ and another in the asymp-

totic region of the quantum well, e.g. near $x = L/2$. For an electron incident at an energy $E > \delta'_{k_y}/2$, conservation laws require $j_{\rm c}|_{x=-\infty} = j_{\rm c}|_{x=L/2} + j_{\rm s}^{\rm sat}$ and $j_{\rm v}|_{x=-\infty} = j_{\rm v}|_{x=L/2} - j_{\rm s}^{\rm sat}$. For transport through conduction quasiparticle channel, $j_{\rm c}|_{x=-\infty} = j_{\rm in} = j$ and $j_{\rm v}|_{x=-\infty} = 0$. Using the relation $(j_{\rm c}/j_{\rm v})_{x=L/2} = -u_{\mathbf{k}}^2/v_{\mathbf{k}}^2$, we have $j_s^{\rm sat} = j_{\rm v}|_{x=L/2}$ and

$$\frac{j_{\rm s}^{\rm sat}}{j} = -\frac{v_{\mathbf{k}}^2}{u_{\mathbf{k}}^2 - v_{\mathbf{k}}^2} \equiv \alpha_{\mathbf{k}}, \tag{4.5}$$

where $u_{\mathbf{k}}$ and $v_{\mathbf{k}}$ are the coherence factors. Because $u_{\mathbf{k}} - v_{\mathbf{k}} > 0$, the minus sign indicate the direction of supercurrent density $j_{\rm s}$ is opposite to the particle current density j.

We calculate the total charge current density in the contact using the Landauer-Büttiker formula

$$I_{tot} = \frac{-e}{hL_y} \sum_{k_y} \int T(E, k_y) \big[f(E - e\tilde{V}_b) - f(E) \big] dE \tag{4.6}$$

where $e > 0$ is the unit of electric charge and $f(E) = 1/[e^{-(E-\mu_R)/k_B T}]$ the Fermi distribution function. Because the Schrödinger equation is time-independent in the rotating frame, We have assumed the chemical potential of the right contact is fixed at the middle of the bandgap $\mu_R = 0$ while $\mu_L = eV_b > 0$ varies. The Schrödinger equation is time-independent in the rotating frame in which the time-dependence $e^{i\omega t}$ is gauded away. The effective bias voltage $\tilde{V}_b$ in the rotating frame is related to the actual bias voltage V_b via $e\tilde{V}_b = eV_b - \hbar\omega$. We calculate the saturated supercurrent from Eq.(4.5)

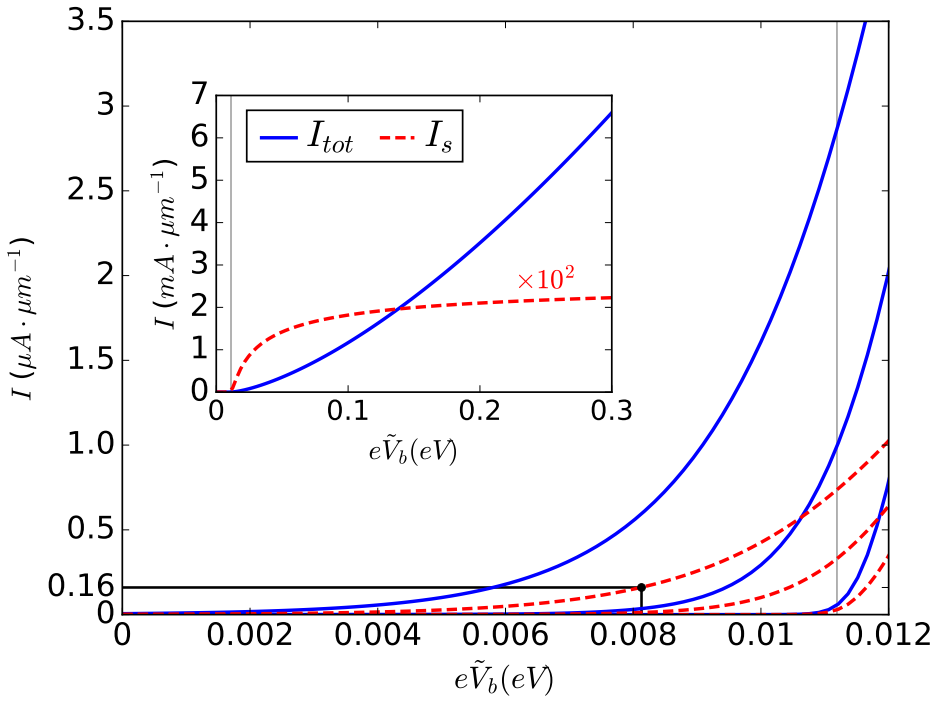

Figure 4.4: (Color online) Current-voltage characteristics at temperatures $T = 2K$, $10K$ and $20K$ (increasing from bottom to top.) $\tilde{V}$ is the effective bias voltage in the rotating frame. The gray line marks the threshold at the quasiparticle gap $e\tilde{V} = \delta_0'/2$.

and Eq.(4.6) which yield

$$I_{\rm s} = \frac{e}{hL_y}\sum_{k_y}\int T(E,k_y)\alpha(E)\big[f(E-e\tilde{V}_b)-f(E)\big]dE \qquad (4.7)$$

where we have arbitrarily multiplied the exciton number current by e in order to place both currents in the same units. Here $\alpha_{\mathbf{k}} = \alpha(E_{\mathbf{k}})$ is independent of k_y and vanishes at energies far above the band gap. As a consequence, when the voltage is increased, the supercurrent will at first increase gradually, before saturating at higher voltages. (See the inset of Fig. 4.4.) The supercurrent I_s

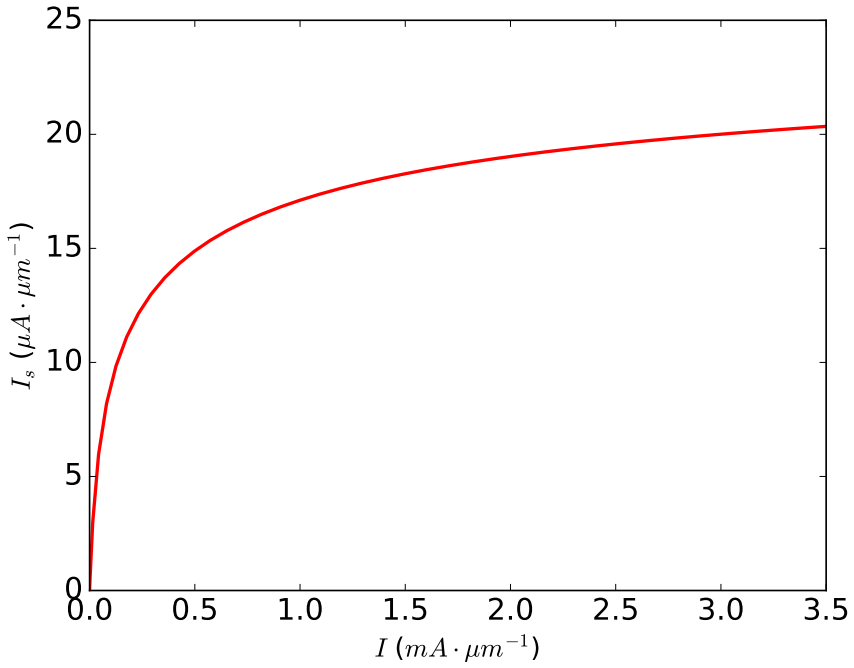

Figure 4.5: (Color online) Supercurrent as a function of total charge current at $T = 2K$. The parameters used here are the same as in Fig.(4.4)

is plotted as a function of the total input charge current I_{tot} in Fig. 4.5. At low bias voltages, I_s increases linearly with I_{tot} with a slope proportional to the exciton density n_{ex}. When the bias moves deep into the conduction band, I_s saturates, in agree with the saturation shown in the $I - V$ curve.

4.3 Exciton-photon transfer

In this section, we address the length scale over which the exciton supercurrent is converted to a lower polariton supercurrent. The large value of this length scale compared to the length scale on which the exciton super-

current is generated justifies our simplified two-step model. To identify this length scale, we turn to the bosonic description of coupled coherent exciton $\Phi_{\rm ex}$ and coherent photon $\Phi_{\rm ph}$ fields. These are described by the coupled linear Gross-Pitaevskii equations [22, 63]

$$\hbar\omega\Phi_{\rm ex}(\mathbf{r}) = \left[-\frac{\hbar^2\nabla^2}{2m_{\rm ex}} + \epsilon^0_{\rm ex}\right]\Phi_{\rm ex}(\mathbf{r}) + \Omega(x)\Phi_{\rm ph}(\mathbf{r}) \tag{4.8}$$

$$\hbar\omega\Phi_{\rm ph}(\mathbf{r}) = \left[-\frac{\hbar^2\nabla^2}{2m_{\rm ph}} + \hbar\omega_0\right]\Phi_{\rm ph}(\mathbf{r}) + \Omega(x)\Phi_{\rm ex}(\mathbf{r}), \tag{4.9}$$

where we have neglected the weak nonlinear term that accounts for exciton-exciton interactions and assumed that the condensate is in a quasi-equilibrium in which compensating pump and decay terms can be ignored. We focus on the right boundary of the cavity where the exciton supercurrent is generated and flows towards left boundary and define the cavity region by imposing a step-like profile on the Rabi coupling: $\Omega(x) = \Theta(L-x)\Omega_0$. The reverse process at the left boundary region can be considered in a similar fashion. In the bulk, the resonant coupling between exciton and photon modes produces two new eigen-branches, the lower polariton(LP) and the upper polariton(UP), which have quadratic dispersion around zero momentum and effective masses $m^{-1}_{\rm UP/LP} \approx m^{-1}_{\rm ph}\big[1 \pm (\hbar\omega_0 - \epsilon^0_{\rm ex})/\sqrt{(\hbar\omega_0 - \epsilon^0_{\rm ex})^2 + 4\Omega^2}\,\big]/2$.

At $x = L^-$ the exciton component of the condensate carries a finite supercurrent. The condensate may also have a photon component which does not carry a current. When the condensate is decomposed into UP and LP components, and the condensate has formed with a chemical potential $\hbar\omega$ near the bottom of the LP branch, its UP component is evanescent. Because Rabi

coupling conserves total boson number while allowing for conversion between excitons and photons, total polariton current is identical with the exciton supercurrent generated at first step. It follows that the exciton supercurrent generated by quasiparticle-condensate transfer at the boundary of the coherent region is identical to the polariton supercurrent carried in the bulk of the coherent region where the ratio between photon and exciton parts of the condensate is that of the LP mode. The length scale over which the LP form of the condensate is recovered is the decay length λ_{UP} of the evanescent upper polariton (UP) wave which satisfies

$$\lambda_{UP}^{-2} = \frac{2m_{\mathrm{UP}}\sqrt{(\hbar\omega_0 - \epsilon_{\mathrm{ex}}^0)^2 + 4\Omega^2}}{\hbar^2} \tag{4.10}$$

assuming that $\hbar\omega$ is close to the LP band bottom. Given the typical detuning $\hbar\omega_0 - \epsilon_{\mathrm{ex}}^0 \sim 10\mathrm{meV}$ and Rabi coupling $\Omega \sim 10\mathrm{meV}$ values we estimate that $\lambda \sim 200\mathrm{nm}$. Generally $\lambda^2/\xi^2 \approx m_0/m_{\mathrm{ph}} \sim 10^4$, provided that the renormalized gap δ_0' and the UP-LP splitting $\sqrt{(\hbar\omega_0 - \epsilon_{\mathrm{ex}}^0)^2 + 4\Omega^2}$ are similar in magnitude. This large ration validates our simplification of the electronic to polaritonic current conversion process into two steps occurring sequentially in space.

4.4 Condensate momentum in the superfluid state

When it carries a supercurrent the condensate has a non-zero phase gradient. As explained above, over the bulk of the coherent region we expect a pure LP condensate with uniform density and phase gradient, i.e. $\Phi_{\mathrm{LP}}(\mathbf{r}, t) = \phi_{\mathrm{LP}} e^{i(k_s x - \omega t)}$ where k_s is the condensate momentum in the x direction. The

condensate momentum and current density are related by

$$I_{\mathrm{s}} = e n_{\mathrm{s}} v_{\mathrm{s}} \tag{4.11}$$

where $n_{\mathrm{s}} = |\phi_{\mathrm{LP}}|^2$ is the density and $v_{\mathrm{s}} = \hbar k_{\mathrm{s}}/m_{\mathrm{LP}}$ the superfluid velocity of the LP condensate. Owing to the dynamic nature of polariton condensates, photons are emitted continuously out of the cavity, carrying precise information about the momentum space distribution of the parent polariton particles [26, 42]. The condensate momentum k_s can thus be measured using angle-resolved emission spectroscopy. At zero bias, the quasi-equilibrium condensate can either be formed spontaneously at zero momentum using a standard non-resonant pumping scheme, or pumped directly with a resonant laser pump at finite momentum $k_s \neq 0$. When an electrical bias is applied, k_s is shifted with respect to the unbiased ground state and the emitted photons acquire an extra transverse momentum $\Delta k = k_s$.

Quasiparticle-condensate transfer can be observed if a detectable momentum shift Δk is achievable. Because of their finite size, even deep in the condensate regime, polariton condensates have a finite width in their momentum distribution, which places a fundamental limit on the resolution of the condensate momentum k_s. It has been shown that the $1/e$ width (or the FWHM) of the momentum distribution above the threshold pumping density is typically 0.5 to $1\mu m^{-1}$ [27, 28, 59]. As the pumping density increases, the momentum distribution broadens slightly possibly due to polariton-polariton interactions. Taking the minimum detectable k_s interval as $\Delta k^{\mathrm{min}} \sim 1\mu m^{-1}$

and using Eq.(4.11), we estimate that the corresponding LP supercurrent density for $k_s = \Delta k^{\min}$ is,

$$I_{\rm s}^{\min} \approx 1.6 \times 10^{-1} \mu A \cdot \mu m^{-1} \tag{4.12}$$

where we have taken $m_{\rm LP} = 10^{-4} m_0$ and $n_{\rm LP} = 1 \mu m^{-2}$, which is slightly larger than the threshold density. We have marked the bias voltage at which $I_{\rm s}^{\min}$ is reached on the $I_{\rm s} - V$ curve in Fig. 4.4. The required voltage is well in the sub-gap regime in which the transport is mainly due to the tail of the Fermi distribution.

4.5 Summary and discussion

In this article we have described a mechanism by which an electrical bias voltage applied across a unipolar semiconductor quantum well can drive an exciton or polariton supercurrent, and illustrated using a simplified model calculation that assumes ballistic transport and abrupt boundaries between a cavity region in which a polariton condensate is established. Our mechanism is based on spatially inhomogeneous mixing between conduction and valence bands in quantum wells or two-dimensional materials when they are dressed by interactions with the coherent exciton and photon fields of a polariton condensate. Because of this dressing, the mean-field Hamiltonian of the quasiparticles, unlike the microscopic Hamiltonian, does not conserve particle number in conduction and valence bands separately. The conservation law is restored by the action of the quasiparticles on the condensate, and this action

is the source which generates an exciton supercurrent. A similar mechanism applies to pure excitonic condensates, and indeed is thought to produce an excitonic supercurrent when a charge current flows through the strong-field quantum-Hall excitonic condensate state of bilayer electron systems [31]. In the polariton case, unlike the quantum Hall case, the supercurrent can in principle be directly measured by examining the photons that leak out of the cavity. According to a qualitative estimate based on the simplified model calculation, the effect is strong enough to produce a measurable condensate momentum shift.

The polariton steady state in the presence of an electronic bias voltage should in principle be determined by solving coupled mean-field equations that differ from those described in Ref. [87] only because the fermionic quasiparticles are in contact with source and drain reservoirs that have different chemical potentials. In such a calculation, the finite momentum of the polariton would emerge naturally from the self-consistent calculation. A similar calculation has been performed previously [73] for a model excitonic condensate. In the present case we have simplified the calculation by assuming a two step process in which the condensate current is generated very close to the boundary of the coherent region, and that it is transformed by Rabi coupling into a purely lower-polariton condensate current over a longer length scale. This simplification allows us to ignore the finite momentum of the condensate when we calculate the conduction and valence band contributions to the quasiparticle current, and is justified by the large difference between the length scales of the

two processes.

The process by which a quasiparticle current driven through a polariton condensate generates a polariton supercurrent is partly analogous to the process by which a quasiparticle current driven through a normal-superconductor-normal metallic circuit generates a supercurrent in the superconducting metal. Andreev scattering is a process which involves change of band character of the outgoing particle. In the case of a metal-superconductor junction, broken particle-number conservation in the mean-filed Hamiltonian allows both Andreev reflection (AR), a process in which an incident electron is reflected as a hole on the normal-metal side of the junction, and Andreev transmission (AT), a process in which an incident electron is transmitted into the superconductor with partial hole-like character. Because the contacts are n-type, the model we have studied for polariton condensation does not allow the analog of AR and AT but the normal transmission (NT) channel involving the dressed conduction quasiparticle band. The violation of particle-number conservation is weaker in the polariton case because the dressed conduction bands are still dominantly conduction band in character, but the effect that launches a Cooper-pair supercurrent in a superconductor is still similar to the effect discussed here.

The simplified model we have used above to illustrate our quasiparticle-condensate effect assumes ballistic scattering. Even in samples that are completely free of disorder, this assumption is not realistic. For example, the high-energy electrons emitted from the source can scatter by emitting phonons.

Even more important, the scenario we are imagine here requires some separate process, whether optical or electronic, that creates a population of conduction band electrons and valence band holes that supports the polariton condensate steady state. Electronic quasiparticles will scatter off these electrons or holes, or off the population of non-resonant excitons that appears when they form bound states. Scattering is important in limiting the amount of charge current that can flow through the system at a given bias voltage. Because the supercurrent is generated immediately upon entry of the quasiparticles into the coherent region, however, we do not expect that the amount of supercurrent generated for a given charge current will differ greatly from the estimate we have obtained.

Quasiparticle-condensate transfer can be used to deflect polariton supercurrents providing, for example the possibility of electrical control of polariton flow at junctions. Because Rabi coupling converts the condensate current to a lower polariton current, and the lower polariton state is in general spread across a number of quantum wells or two-dimensional material layers, the dressed quasiparticle Hamiltonian in one layer can be influenced by bias voltages applied to another layer separated by some number of photon wavelengths. We anticipate that the effect we have described might therefore enable interesting possibilities for coherent electrical coupling between two-dimensional electron systems separated by micron length scales.

Appendix

Appendix A

Equation of motion formalism for exciton-photon transfer

This chapter derives the equation of motion of density operators and field operators which explicitly show the terms that are responsible for the conversion between the excitonic and the photonic components of the supercurrent in polariton condensates.

A.1 Microscopic Hamiltonian

The microscopic Hamiltonian of a microcavity-quantum-well system in terms of real space field operators writes:

$$\hat{H} = \sum_{\alpha=c,v} \int \Psi_\alpha^\dagger(\mathbf{r}) \hat{h}_\alpha \Psi_\alpha(\mathbf{r}) d\mathbf{r} + \frac{1}{2} \sum_{\alpha,\beta} \int V(\mathbf{r}_1 - \mathbf{r}_2) \Psi_\alpha^\dagger(\mathbf{r}_1) \Psi_\beta^\dagger(\mathbf{r}_2) \Psi_\beta(\mathbf{r}_2) \Psi_\alpha(\mathbf{r}_1) d\mathbf{r}_1 d\mathbf{r}_2 + \frac{I_z|e|}{mc} \sum_{\alpha \neq \beta} \int \Psi_\alpha^\dagger(\mathbf{r}) \hat{\mathbf{A}}(\mathbf{r}) \cdot \hat{\mathbf{p}} \Psi_\beta(\mathbf{r}) d\mathbf{r} + \frac{1}{2} \int \left(\epsilon \dot{\hat{\mathbf{A}}}(\mathbf{r})^2 + \frac{1}{\mu} \left[\nabla \times \hat{\mathbf{A}}(\mathbf{r}) \right]^2 \right) d\mathbf{r} \tag{A.1}$$

where $\Psi_\alpha(\mathbf{r})$ is electron field operator and $\alpha, \beta = c, v$ represent conduction and valence band indices. $\mathbf{r}$ is a 2-dimensional vector. $\hat{\mathbf{A}}$ is the vector potential whose fast frequency component is neglected in rotating wave approximation.

The non-interacting Hamiltonian is

$$\hat{h}_{c(v)} = \pm\left(-\frac{\hbar^2\nabla^2}{2m} + \frac{\delta}{2}\right)$$

with $\delta = E_g - \hbar\omega$ the reduced gap in the rotating frame. The second term is the electron-electron Coulomb interaction.

The third terms is the electron-photon coupling term. One thing that comes in determining the e-ph coupling strength is the overlap integral of envelop functions in z-direction

$$I_z = \int f_c(z) f_v(z) A(z) dz \tag{A.2}$$

where $f_{c(v)}(z)$ is the envelop function for conduction (valence) band state and $A(z)$ that of photons as in $A(\boldsymbol{r}) \equiv A(x,y)A(z)$.

The dipole formed by the e-h pair couples to TM mode of electromagnetic field since the E-field component of TM mode is paralle to the xy plane $\boldsymbol{\epsilon}_{TM} \cdot \boldsymbol{p} \neq 0$ while that of TE mode are perpendicular to xy plane, $\boldsymbol{\epsilon}_{TE} \cdot \boldsymbol{p} = 0$. We focus on this TM mode and reduce the vector field to a scalar field:

$$\hat{\mathbf{A}}(\mathbf{r}) \to \left[\Phi_{\text{ph}}(\mathbf{r}) + \Phi^{\dagger}_{\text{ph}}(\mathbf{r})\right] \boldsymbol{\epsilon}_{TM} \tag{A.3}$$

when substituting into the 3rd term, we will ignore the fast frequency term accordingly in the spirit of *rotating wave approximation* and get the $H_{\text{e-ph}}$ term in the following Hamiltonian Eq. (A.5).

The fourth term gives the usual kinetic energy term H_{ph} in the following Hamiltonian Eq. (A.5).

By approximating the electron-photon coupling using a momentum independent coupling constant

$$g = \frac{I_z|e|}{mc} \tag{A.4}$$

and expanding the kinetic energy for photons to quadratic order near small photon wave-vectors, the Hamiltonian (A.1) can be rewritten as:

$$\begin{aligned}\hat{H} = &\underbrace{\sum_{\alpha=c,v}\int \Psi^\dagger_\alpha(\mathbf{r})\hat{h}_\alpha\Psi_\alpha(\mathbf{r})d\mathbf{r}}_{\hat{H}_0} + \underbrace{\frac{1}{2}\sum_{\alpha,\beta}\int V(\mathbf{r}_1-\mathbf{r}_2)\Psi^\dagger_\alpha(\mathbf{r}_1)\Psi^\dagger_\beta(\mathbf{r}_2)\Psi_\beta(\mathbf{r}_2)\Psi_\alpha(\mathbf{r}_1)d\mathbf{r}_1 d\mathbf{r}_2}_{\hat{H}_{\text{int}}} \\ &+ \underbrace{g\int\left(\Phi_{\text{ph}}(\mathbf{r})\Psi^\dagger_c(\mathbf{r})\Psi_v(\mathbf{r}) + \Phi^\dagger_{\text{ph}}(\mathbf{r})\Psi^\dagger_v(\mathbf{r})\Psi_c(\mathbf{r})\right)d\mathbf{r}}_{\hat{H}_{\text{el-ph}}} + \underbrace{\int\Phi^\dagger_{\text{ph}}(\mathbf{r})\left(\hbar\omega_0 - \frac{\hbar^2\nabla^2}{2m_{\text{ph}}}\right)\Phi_{\text{ph}}(\mathbf{r})d\mathbf{r}}_{\hat{H}_{\text{ph}}}\end{aligned} \tag{A.5}$$

The equation of motion of the density operator can be obtained from the Heisenberg equation as follows:

$$\dot{\hat{n}}_\alpha = \frac{i}{\hbar}[\hat{H}, \hat{n}_\alpha] \tag{A.6}$$

Below, I calculate the commutators of $\hat{n}_\alpha$ with each term of the Hamiltonian:

$$
\begin{aligned}
[\hat{H}_0, \hat{n}_\alpha(\mathbf{r})] &= \sum_\beta \int d\mathbf{r}' \cdot [\Psi^\dagger_\beta(\mathbf{r}')\hat{h}_\beta\Psi_\beta(\mathbf{r}'), \Psi^\dagger_\alpha(\mathbf{r})\Psi_\alpha(\mathbf{r})] \\
&= -\sum_\beta \frac{\hbar^2}{2m_\beta} \int d\mathbf{r}' \left[\Psi^\dagger_\beta(\mathbf{r}')\nabla^2\Psi_\beta(\mathbf{r}'), \Psi^\dagger_\alpha(\mathbf{r})\Psi_\alpha(\mathbf{r})\right] \\
&= -\sum_\beta \frac{\hbar^2}{2m_\beta} \int d\mathbf{r}' \left(-\Psi^\dagger_\alpha(\mathbf{r})\delta_{\alpha\beta}\delta(\mathbf{r}-\mathbf{r}')\nabla^2\Psi_\beta(\mathbf{r}') + \Psi^\dagger_\beta(\mathbf{r}')\delta_{\alpha\beta}\nabla^2\delta(\mathbf{r}-\mathbf{r}')\cdot\Psi_\alpha(\mathbf{r})\right) \\
&= -\frac{\hbar^2}{2m_\alpha}\left[\left(\nabla^2\Psi^\dagger_\alpha(\mathbf{r})\right)\Psi_\alpha(\mathbf{r}) - \Psi^\dagger_\alpha(\mathbf{r})\nabla^2\Psi_\alpha(\mathbf{r})\right] \\
&= -\frac{\hbar^2}{2m_\alpha}\nabla\cdot\left[\left(\nabla\Psi^\dagger_\alpha(\mathbf{r})\right)\Psi_\alpha(\mathbf{r}) - \Psi^\dagger_\alpha(\mathbf{r})\nabla\Psi_\alpha(\mathbf{r})\right] \\
&= i\hbar\nabla\cdot\hat{j}_\alpha
\end{aligned}
\tag{A.7}
$$

where for simplicity we have defined $m_c = m_0$ and $m_v = -m_0$. We also defined the probability current operator as

$$
\hat{j}_\alpha(\boldsymbol{r}) \equiv \frac{i\hbar}{2m_\alpha}\left[\left(\nabla\Psi^\dagger_\alpha(\mathbf{r})\right)\Psi_\alpha(\mathbf{r}) - \Psi^\dagger_\alpha(\mathbf{r})\nabla\Psi_\alpha(\mathbf{r})\right]. \tag{A.8}
$$

Commutator with electron-electron interaction Hamiltonian:

$$
\begin{aligned}
[\hat{H}_{\text{int}}, \hat{n}_\alpha(\mathbf{r})] &= \frac{1}{2}\sum_{\gamma,\beta}\int V(\mathbf{r}_1-\mathbf{r}_2)d\mathbf{r}_1 d\mathbf{r}_2\left[\Psi^\dagger_\gamma(\mathbf{r}_1)\Psi^\dagger_\beta(\mathbf{r}_2)\Psi_\beta(\mathbf{r}_2)\Psi_\gamma(\mathbf{r}_1), \Psi^\dagger_\alpha(\mathbf{r})\Psi_\alpha(\mathbf{r})\right] \\
&= 0
\end{aligned}
\tag{A.9}
$$

The contribution from electron-photon coupling:

$$
\begin{aligned}
&[\hat{H}_{\text{el-ph}}, \hat{n}_\alpha(\mathbf{r})] \\
&= g \int d\mathbf{r}' \left[\Phi_{\text{ph}}(\mathbf{r}')\Psi_c^\dagger(\mathbf{r}')\Psi_v(\mathbf{r}') + \Phi_{\text{ph}}^\dagger(\mathbf{r}')\Psi_v^\dagger(\mathbf{r}')\Psi_c(\mathbf{r}'), \Psi_\alpha^\dagger(\mathbf{r})\Psi_\alpha(\mathbf{r}) \right] \\
&= g\Phi_{\text{ph}}(\mathbf{r}) \left(\Psi_c^\dagger(\mathbf{r})\Psi_\alpha(\mathbf{r})\delta_{\alpha v} - \Psi_\alpha^\dagger(\mathbf{r})\Psi_v(\mathbf{r})\delta_{\alpha c} \right) \\
&\quad + g\Phi_{\text{ph}}^\dagger(\mathbf{r}) \big(\Psi_v^\dagger(\mathbf{r})\Psi_\alpha(\mathbf{r})\delta_{\alpha c} - \Psi_\alpha^\dagger(\mathbf{r})\Psi_c(\mathbf{r})\delta_{\alpha v} \big)
\end{aligned} \tag{A.10}
$$

and it is easy to see

$$
[\hat{H}_{\text{ph}}, \hat{n}_\alpha] = 0 \tag{A.11}
$$

For $\hat{n}_{\text{ph}}$, we have $[\hat{H}_0, \hat{n}_{\text{ph}}] = 0$ and $[\hat{H}_{\text{int}}, \hat{n}_{\text{ph}}] = 0$. The non-vanishing terms are from the coupling term

$$
\begin{aligned}
[\hat{H}_{\text{el-ph}}, \hat{n}_{\text{ph}}(\mathbf{r})] &= g \int d\mathbf{r}' \left[\Phi_{\text{ph}}(\mathbf{r}')\Psi_c^\dagger(\mathbf{r}')\Psi_v(\mathbf{r}') + \Phi_{\text{ph}}^\dagger(\mathbf{r}')\Psi_v^\dagger(\mathbf{r}')\Psi_c(\mathbf{r}'), \Phi_{\text{ph}}^\dagger(\mathbf{r})\Phi_{\text{ph}}(\mathbf{r}) \right] \\
&= g \int d\mathbf{r}' \left(\Phi_{\text{ph}}(\mathbf{r})\delta(\mathbf{r}-\mathbf{r}')\Psi_c^\dagger(\mathbf{r}')\Psi_v(\mathbf{r}') + \Phi_{\text{ph}}^\dagger(\mathbf{r})\delta(\mathbf{r}-\mathbf{r}')\Psi_v^\dagger(\mathbf{r}')\Psi_c(\mathbf{r}') \right) \\
&= g \left(\Phi_{\text{ph}}(\mathbf{r})\Psi_c^\dagger(\mathbf{r})\Psi_v(\mathbf{r}) - \Phi_{\text{ph}}^\dagger(\mathbf{r})\Psi_v^\dagger(\mathbf{r})\Psi_c(\mathbf{r}) \right)
\end{aligned} \tag{A.12}
$$

and the kinetic energy term

$$
\begin{aligned}
[\hat{H}_{\text{ph}}, \hat{n}_{\text{ph}}(\mathbf{r})] &= \int d\mathbf{r}' [\Phi_{\text{ph}}^\dagger(\mathbf{r}') \left(\hbar\omega_0 - \frac{\hbar^2\nabla^2}{2m_{\text{ph}}} \right) \Phi_{\text{ph}}(\mathbf{r}'), \Phi_{\text{ph}}^\dagger(\mathbf{r})\Phi_{\text{ph}}(\mathbf{r})] \\
&= -\frac{\hbar^2}{2m_{\text{ph}}} \nabla \cdot \left[\left(\nabla\Phi_{\text{ph}}^\dagger(\mathbf{r}) \right) \Phi_{\text{ph}}(\mathbf{r}) - \Phi_{\text{ph}}^\dagger(\mathbf{r}) \nabla\Phi_{\text{ph}}(\mathbf{r}) \right] \\
&= i\hbar\nabla \cdot \hat{j}_{\text{ph}}(\boldsymbol{r})
\end{aligned} \tag{A.13}
$$

where we defined the photon current operator

$$
\hat{j}_{\text{ph}}(\boldsymbol{r}) \equiv \frac{i\hbar}{2m_{\text{ph}}} \left[\big(\nabla\Phi_{\text{ph}}^\dagger(\mathbf{r}) \big) \Phi_{\text{ph}}(\mathbf{r}) - \Phi_{\text{ph}}^\dagger(\mathbf{r}) \nabla\Phi_{\text{ph}}(\mathbf{r}) \right] \tag{A.14}
$$

Collecting all the commutators we get

$$\dot{\hat{n}}_c = -\nabla \cdot \hat{j}_c - \frac{ig}{\hbar}\left(\Phi_{\rm ph}(\mathbf{r})\Psi_c^\dagger(\mathbf{r})\Psi_v(\mathbf{r}) - \Phi_{\rm ph}^\dagger(\mathbf{r})\Psi_v^\dagger(\mathbf{r})\Psi_c(\mathbf{r})\right) \tag{A.15}$$

$$\dot{\hat{n}}_v = -\nabla \cdot \hat{j}_v + \frac{ig}{\hbar}\left(\Phi_{\rm ph}(\mathbf{r})\Psi_c^\dagger(\mathbf{r})\Psi_v(\mathbf{r}) - \Phi_{\rm ph}^\dagger(\mathbf{r})\Psi_v^\dagger(\mathbf{r})\Psi_c(\mathbf{r})\right) \tag{A.16}$$

$$\dot{\hat{n}}_{\rm ph} = -\nabla \cdot \hat{j}_{\rm ph} + \frac{ig}{\hbar}\left(\Phi_{\rm ph}(\mathbf{r})\Psi_c^\dagger(\mathbf{r})\Psi_v(\mathbf{r}) - \Phi_{\rm ph}^\dagger(\mathbf{r})\Psi_v^\dagger(\mathbf{r})\Psi_c(\mathbf{r})\right) \tag{A.17}$$

In connection with the wave-function $f(\boldsymbol{r},t)$ and $g(\boldsymbol{r},t)$ for conduction and valence component of the quasiparticle, we have

$$f(\boldsymbol{r},t) = \langle\phi_G|\Psi_c(\boldsymbol{r},t)|\phi^e\rangle \tag{A.18}$$

$$g(\boldsymbol{r},t) = \langle\phi_G|\Psi_v(\boldsymbol{r},t)|\phi^e\rangle \tag{A.19}$$

where $|\phi_G\rangle$ is the condensate ground state with no quasiparticle excitation and $|\phi^e\rangle$ is the excited states with one quasiparticle added to the ground state. We also note the following relation:

$$\left(\nabla f^*(\boldsymbol{r},t)\right) f(\boldsymbol{r},t) = \langle\phi_G|\left(\nabla\Phi_{\rm c}^\dagger(\mathbf{r})\right)\Psi_c(\boldsymbol{r},t)|\phi^e\rangle \tag{A.20}$$

By taking expectation value of above equation of motions Eq. (A.15-A.17), we get

$$\frac{\partial\rho_c}{\partial t} + \nabla\cdot j_c = \frac{2g\psi_{\rm ph}}{\hbar}{\rm Im}\left[f^*g\right] \tag{A.21}$$

$$\frac{\partial\rho_v}{\partial t} + \nabla\cdot j_v = -\frac{2g\psi_{\rm ph}}{\hbar}{\rm Im}\left[f^*g\right] \tag{A.22}$$

$$\frac{\partial\rho_{\rm ph}}{\partial t} + \nabla\cdot j_{\rm ph} = \frac{2g\psi_{\rm ph}}{\hbar}{\rm Im}\left[f^*g\right] \tag{A.23}$$

A.2 Equation of motion from the mean-field Hamiltonian

We derive the equation of motion starting from mean field Hamiltonian which approximates the electron-electron interaction term by

$$\hat{H}_{\text{int}} \rightarrow \hat{H}_{\text{int}}^{\text{MF}} \tag{A.24}$$

which includes only the interband exchange part

$$\hat{H}_{\text{int}}^{\text{MF}} = \int \left(\Delta(\mathbf{r}_1, \mathbf{r}_2) \hat{\Psi}_{\text{c}}^{\dagger}(\mathbf{r}_2) \hat{\Psi}_{\text{v}}(\mathbf{r}_1) + \Delta^*(\mathbf{r}_1, \mathbf{r}_2) \hat{\Psi}_{\text{v}}^{\dagger}(\mathbf{r}_2) \hat{\Psi}_{\text{c}}(\mathbf{r}_1) \right) d\mathbf{r}_1 d\mathbf{r}_2 \tag{A.25}$$

The exciton mean field is defined as

$$\begin{aligned} \Delta(\mathbf{r}_1, \mathbf{r}_2) &= V(\mathbf{r}_1 - \mathbf{r}_2) \langle \hat{\Psi}_{\text{c}}(\mathbf{r}_1) \hat{\Psi}_{\text{v}}^{\dagger}(\mathbf{r}_2) \rangle \\ \Delta^*(\mathbf{r}_1, \mathbf{r}_2) &= V(\mathbf{r}_1 - \mathbf{r}_2) \langle \hat{\Psi}_{\text{v}}(\mathbf{r}_2) \hat{\Psi}_{\text{c}}^{\dagger}(\mathbf{r}_1) \rangle \end{aligned} \tag{A.26}$$

The total Hamiltonian now becomes

$$\hat{H}^{\text{MF}} = \hat{H}_0 + \hat{H}_{\text{int}}^{\text{MF}} + \hat{H}_{\text{el-ph}} + \hat{H}_{\text{ph}} \tag{A.27}$$

The commutator of the density operator $\hat{n}_c$with the exchange term can be derived as

$$\begin{aligned} &[\hat{H}_{\text{int}}^{\text{MF}}, \hat{n}_c(\mathbf{r})] \\ &= \int d\mathbf{r}_1 d\mathbf{r}_2 \left[\Delta(\mathbf{r}_1, \mathbf{r}_2) \hat{\Psi}_{\text{c}}^{\dagger}(\mathbf{r}_2) \hat{\Psi}_{\text{v}}(\mathbf{r}_1) + \Delta^*(\mathbf{r}_1, \mathbf{r}_2) \hat{\Psi}_{\text{v}}^{\dagger}(\mathbf{r}_2) \hat{\Psi}_{\text{c}}(\mathbf{r}_1), \Psi_c^{\dagger}(\mathbf{r}) \Psi_c(\mathbf{r}) \right] \\ &= - \int d\mathbf{r}_1 d\mathbf{r}_2 \left[\Delta(\mathbf{r}_1, \mathbf{r}_2) \hat{\Psi}_{\text{c}}^{\dagger}(\mathbf{r}_2) \hat{\Psi}_{\text{v}}(\mathbf{r}_1) \delta(\mathbf{r} - \mathbf{r}_2) - \Delta^*(\mathbf{r}_1, \mathbf{r}_2) \hat{\Psi}_{\text{v}}^{\dagger}(\mathbf{r}_2) \hat{\Psi}_{\text{c}}(\mathbf{r}_1) \delta(\mathbf{r} - \mathbf{r}_1) \right] \end{aligned} \tag{A.28}$$

Assuming a uniform condensate and neglect the momentum dependence of the interband coherence field, we thus can write it in real space as a delta function:

$$\Delta(\mathbf{r}_1, \mathbf{r}_2) = \Delta_0(\boldsymbol{r}_1)\delta(\mathbf{r}_1 - \mathbf{r}_2) \tag{A.29}$$

Under this assumption, the commutator simplifies to:

$$[\hat{H}^{\mathrm{MF}}_{\mathrm{int}}, \hat{n}_c(\mathbf{r})] = -\left[\Delta(\mathbf{r})\hat{\Psi}^{\dagger}_{\mathrm{c}}(\mathbf{r})\hat{\Psi}_{\mathrm{v}}(\mathbf{r}) - \Delta^*(\mathbf{r})\hat{\Psi}^{\dagger}_{\mathrm{v}}(\mathbf{r})\hat{\Psi}_{\mathrm{c}}(\mathbf{r})\right] \tag{A.30}$$

Replacing the photon field operator with a complex mean-field amplitude leads to

$$\dot{\hat{n}}_c = -\nabla\cdot\hat{j}_c - i\left\{\frac{\Delta(\mathbf{r}) + g\Phi_{\mathrm{ph}}(\mathbf{r})}{\hbar}\Psi^{\dagger}_c(\mathbf{r})\Psi_v(\mathbf{r}) - \frac{\Delta^*(\mathbf{r}) + g\Phi^*_{\mathrm{ph}}(\mathbf{r})}{\hbar}\Psi^{\dagger}_v(\mathbf{r})\Psi_c(\mathbf{r})\right\} \tag{A.31}$$

$$\dot{\hat{n}}_v = -\nabla\cdot\hat{j}_v + i\left\{\frac{\Delta(\mathbf{r}) + g\Phi_{\mathrm{ph}}(\mathbf{r})}{\hbar}\Psi^{\dagger}_c(\mathbf{r})\Psi_v(\mathbf{r}) - \frac{\Delta^*(\mathbf{r}) + g\Phi^*_{\mathrm{ph}}(\mathbf{r})}{\hbar}\Psi^{\dagger}_v(\mathbf{r})\Psi_c(\mathbf{r})\right\} \tag{A.32}$$

$$\dot{\hat{n}}_{\mathrm{ph}} = -\nabla\cdot\hat{j}_{\mathrm{ph}} + i\left\{\frac{g\Phi_{\mathrm{ph}}(\mathbf{r})}{\hbar}\Psi^{\dagger}_c(\mathbf{r})\Psi_v(\mathbf{r}) - \frac{g\Phi^*_{\mathrm{ph}}(\mathbf{r})}{\hbar}\Psi^{\dagger}_v(\mathbf{r})\Psi_c(\mathbf{r})\right\} \tag{A.33}$$

As was done in previous section, we take expectation value of above equation of motion and obtain

$$\frac{\partial\rho_c}{\partial t} + \nabla\cdot j_c = \frac{2(g\psi_{\mathrm{ph}} + \Delta)}{\hbar}\mathrm{Im}\left[f^*g\right] \tag{A.34}$$

$$\frac{\partial\rho_v}{\partial t} + \nabla\cdot j_v = -\frac{2(g\psi_{\mathrm{ph}} + \Delta)}{\hbar}\mathrm{Im}\left[f^*g\right] \tag{A.35}$$

$$\frac{\partial\rho_{\mathrm{ph}}}{\partial t} + \nabla\cdot j_{\mathrm{ph}} = \frac{2g\psi_{\mathrm{ph}}}{\hbar}\mathrm{Im}\left[f^*g\right] \tag{A.36}$$

which is different from the result obtained in the previous section. The mean field interband coherence term Δ was absent in the source and drain terms in the latter result.

A.3 Equation of motion of field operators

The microscopic Hamiltonian in terms of real-space field operators writes:

$$\hat{\mathcal{H}} = \hat{\mathcal{H}}_0 + \hat{\mathcal{H}}_{\text{ph}} + \hat{\mathcal{H}}_{\text{int}} + \hat{\mathcal{H}}_{\text{el-ph}} \tag{A.37}$$

where

$$\hat{\mathcal{H}}_0 = \sum_{\alpha=c,v} \int \Psi^\dagger_\alpha(\mathbf{r}) \hat{h}_\alpha \Psi_\alpha(\mathbf{r}) d\mathbf{r} \tag{A.38}$$

$$\hat{\mathcal{H}}_{\text{ph}} = \int \Phi^\dagger_{\text{ph}}(\mathbf{r}) \left(\hbar\omega_0 - \frac{\hbar^2\nabla^2}{2m_{\text{ph}}} \right) \Phi_{\text{ph}}(\mathbf{r}) d\mathbf{r} \tag{A.39}$$

$$\hat{\mathcal{H}}_{\text{int}} = \frac{1}{2} \sum_{\alpha,\beta} \int V(\mathbf{r}_1 - \mathbf{r}_2) \Psi^\dagger_\alpha(\mathbf{r}_1) \Psi^\dagger_\beta(\mathbf{r}_2) \Psi_\beta(\mathbf{r}_2) \Psi_\alpha(\mathbf{r}_1) d\mathbf{r}_1 d\mathbf{r}_2 \tag{A.40}$$

$$\hat{\mathcal{H}}_{\text{el-ph}} = g \int \left(\Phi_{\text{ph}}(\mathbf{r}) \Psi^\dagger_c(\mathbf{r}) \Psi_v(\mathbf{r}) + \Phi^\dagger_{\text{ph}}(\mathbf{r}) \Psi^\dagger_v(\mathbf{r}) \Psi_c(\mathbf{r}) \right) d\mathbf{r} \tag{A.41}$$

where $\Psi_\alpha(\mathbf{r})$ is the electron field operator and $\alpha, \beta = c, v$ represent conduction and valence band indices respectively. $\mathbf{r}$ is the two-dimensional position vector. $\Phi_{\text{ph}}(\mathbf{r})$ is the field operator for photons with a particular polarization set by the cavity structure. $\hat{\mathcal{H}}_0$ is the non-interacting part of the electronic Hamiltonian with

$$\hat{h}_{c(v)} = \pm \left(-\frac{\hbar^2\nabla^2}{2m} + \frac{\delta}{2} \right)$$

where $\delta = E_g - \hbar\omega$ is the reduced gap in the rotating frame as described in the main text. The second term H_{ph} accounts for the kinetic energy of cavity photons. $\hat{\mathcal{H}}_{\text{int}}$ is the electron-electron Coulomb interaction Hamiltonian. $\hat{\mathcal{H}}_{\text{el-ph}}$ is the electron-photon coupling term.

We derive the equation of motion for the field operators using the Heisenberg equation:

$$\frac{\partial}{\partial t}\hat{\Psi}_\alpha(\boldsymbol{r}) = \frac{i}{\hbar}[\hat{\mathcal{H}}, \hat{\Psi}_\alpha(\boldsymbol{r})] \tag{A.42}$$

The results for electron field operators are

$$\frac{\partial}{\partial t}\hat{\Psi}_c(\boldsymbol{r}) = \frac{i\hbar}{2m_c}\nabla^2\hat{\Psi}_c(\boldsymbol{r}) - \frac{i}{\hbar}\sum_\beta \int d\boldsymbol{r}' V(\boldsymbol{r}-\boldsymbol{r}')\hat{\Psi}^\dagger_\beta(\boldsymbol{r}')\hat{\Psi}_\beta(\boldsymbol{r}')\hat{\Psi}_c(\boldsymbol{r}) - \frac{ig}{\hbar}\hat{\Phi}_{\text{ph}}(\boldsymbol{r})\hat{\Psi}_v(\boldsymbol{r}) \tag{A.43}$$

$$\frac{\partial}{\partial t}\hat{\Psi}_v(\boldsymbol{r}) = \frac{i\hbar}{2m_v}\nabla^2\hat{\Psi}_v(\boldsymbol{r}) - \frac{i}{\hbar}\sum_\beta \int d\boldsymbol{r}' V(\boldsymbol{r}-\boldsymbol{r}')\hat{\Psi}^\dagger_\beta(\boldsymbol{r}')\hat{\Psi}_\beta(\boldsymbol{r}')\hat{\Psi}_v(\boldsymbol{r}) + \frac{ig}{\hbar}\hat{\Phi}^\dagger_{\text{ph}}(\boldsymbol{r})\hat{\Psi}_c(\boldsymbol{r}) \tag{A.44}$$

The result for photon field operator is

$$\frac{\partial}{\partial t}\hat{\Psi}_{\text{ph}}(\boldsymbol{r}) = \frac{i\hbar}{2m_{\text{ph}}}\nabla^2\hat{\Psi}_{\text{ph}}(\boldsymbol{r}) - \frac{ig}{\hbar}\Psi^\dagger_v(\mathbf{r})\Psi_c(\mathbf{r}) \tag{A.45}$$

Taking the expectation values of the field operator,

$$u(\boldsymbol{r},t) = \langle\phi_G|\hat{\Psi}_c(\boldsymbol{r},t)|\phi^e\rangle \tag{A.46}$$

$$v(\boldsymbol{r},t) = \langle\phi_G|\hat{\Psi}_v(\boldsymbol{r},t)|\phi^e\rangle \tag{A.47}$$

$$\phi_{\text{ph}}(\boldsymbol{r},t) = \langle\phi_G|\hat{\Phi}_{\text{ph}}(\boldsymbol{r},t)|\phi_G\rangle \tag{A.48}$$

where $|\phi_G\rangle$ is the condensate ground state with no quasiparticle excitation and $|\phi^e\rangle$ is the excited states with one quasiparticle added to the ground state. For

the expectation value of the interacting term, i.e. $\langle\hat{\Psi}^\dagger\hat{\Psi}^\dagger\hat{\Psi}\rangle$ we take the mean field approximation and define the exciton mean field as

$$\Delta(\mathbf{r}_1,\mathbf{r}_2) = V(\mathbf{r}_1-\mathbf{r}_2)\langle\hat{\Psi}_{\rm c}(\mathbf{r}_1)\hat{\Psi}^\dagger_{\rm v}(\mathbf{r}_2)\rangle \tag{A.49}$$

where $\langle\cdots\rangle$ is the expectation value in the mean field ground state. In the low exciton density limit, the internal motion of the electron-hole pair could be ignored and excitons can be treated as a point-like particle, where the wavefunction dependence on the relative coordinate $\boldsymbol{r}-\boldsymbol{r}'$ takes the delta function form, giving

$$\Delta(\boldsymbol{r},\boldsymbol{r}') = \Delta(\boldsymbol{r})\delta(\boldsymbol{r}-\boldsymbol{r}'). \tag{A.50}$$

The equation of motion of the function $u(\boldsymbol{r},t)$ and $v(\boldsymbol{r},t)$ are therefore

$$\frac{\partial}{\partial t}u(\boldsymbol{r}) = \frac{i\hbar}{2m_c}\nabla^2 u(\boldsymbol{r}) - \frac{i}{\hbar}\Delta(\boldsymbol{r})v(\boldsymbol{r}) - \frac{ig}{\hbar}\phi_{\rm ph}(\boldsymbol{r})v(\boldsymbol{r}) \tag{A.51}$$

$$\frac{\partial}{\partial t}v(\boldsymbol{r}) = \frac{i\hbar}{2m_v}\nabla^2 v(\boldsymbol{r}) - \frac{i}{\hbar}\Delta^*(\boldsymbol{r})u(\boldsymbol{r}) - \frac{ig}{\hbar}\phi^*_{\rm ph}(\boldsymbol{r})u(\boldsymbol{r}) \tag{A.52}$$

and similarly for photon field

$$\frac{\partial}{\partial t}\phi_{\rm ph}(\boldsymbol{r}) = \frac{i\hbar}{2m_{\rm ph}}\nabla^2\phi_{\rm ph}(\boldsymbol{r}) - \frac{ig}{\hbar}u(\boldsymbol{r})v^*(\mathbf{r}) \tag{A.53}$$

The equation of motion of probability functions can be easily obtained

$$\frac{\partial}{\partial t}|u(\boldsymbol{r})|^2 = -\nabla j_c(\boldsymbol{r}) + \frac{2}{\hbar}{\rm Im}\{[\Delta(\boldsymbol{r}) + g\phi_{\rm ph}(\boldsymbol{r})]u^*(\boldsymbol{r})v(\boldsymbol{r})\} \tag{A.54}$$

$$\frac{\partial}{\partial t}|v(\boldsymbol{r})|^2 = -\nabla j_v(\boldsymbol{r}) - \frac{2}{\hbar}{\rm Im}\{[\Delta(\boldsymbol{r}) + g\phi_{\rm ph}(\boldsymbol{r})]u^*(\boldsymbol{r})v(\boldsymbol{r})\} \tag{A.55}$$

and for photon

$$\frac{\partial}{\partial t}|\phi_{\rm ph}(\boldsymbol{r})|^2 = -\nabla j_{\rm ph}(\boldsymbol{r}) + \frac{2}{\hbar}{\rm Im}\{g\phi_{\rm ph}(\boldsymbol{r})u^*(\boldsymbol{r})v(\boldsymbol{r})\} \tag{A.56}$$

which is similar to the equation of motion of density operators we obtained in last section.

Appendix B

Nonuniform polariton condensate suppercurent flow

Consider following potential trap for polaritons (Fig. B.1) which includes both a source and a drain at two different locations of the well $x = -a$ and a, respectively. They represent the Andreev type conversion from electrical current to polariton current and vice versa. The wavefunction can be solved provided that the source and the drain have the same strength such that the total number of polaritons is unchanged. This guarantees that eigenenergies are still real. For bound states, polariton current only flow between $(-a, a)$.

The macroscopic condensate wavefunction satisfies the Gross-Pitaevskii equation

$$i\frac{\partial\Psi(x)}{\partial t} = \left(-\frac{\hbar^2}{2m}\frac{\partial^2}{\partial x^2} + \frac{1}{2}m\omega_0^2 x^2 + i\gamma_L\delta(x+a) + i\gamma_R\delta(x-a)\right)\Psi(x) \quad \text{(B.1)}$$

where we have ignored polariton-polariton interaction $g = 0$. It could be included later if we want using numerical method. m is the effective mass of polariton. We also assume $\gamma_L = -\gamma_R = \gamma$.

Because of the delta functions, we need to solve for the wavefunction as a boundary value problem. The boundary condition is of the familiar form

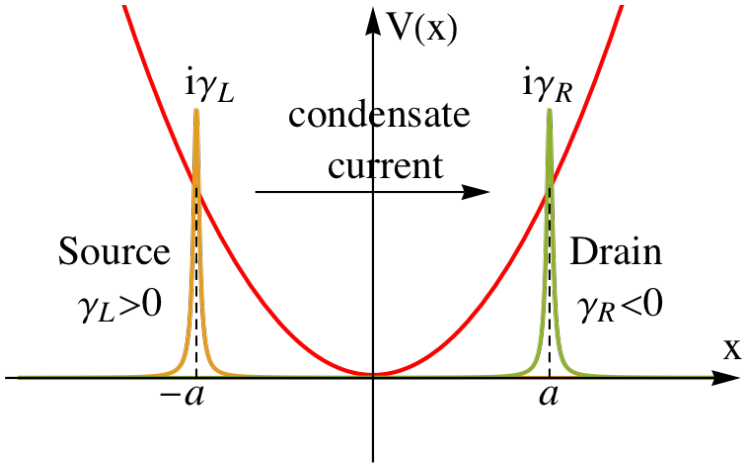

Figure B.1: Schematic plot of the potential trap for polaritons. A source and a drain are included in the form of delta functions located at $-a$ and a respectively. They have imaginary amplitudes with $\gamma_L > 0$ respresenting pumping of polaritons from electrically driven Andreev type conversion and $\gamma_R < 0$ for loss due to the inverse conversion process. We will assume $\gamma_L = -\gamma_R > 0$. The condensate current will flow between $(-a, a)$ only.

for delta function barrier. For example at $x = a$,

$$\Psi(a^+) = \Psi(a^-) \tag{B.2}$$

$$\Psi'(a^+) - \Psi'(a^-) = \frac{2i\gamma m}{\hbar^2} \tag{B.3}$$

On the other hand, the polariton probability current is given by:

$$j(x) = \frac{\hbar}{2im}\left[\Psi^*(x)\Psi'(x) - \Psi^{*\prime}(x)\Psi(x)\right]. \tag{B.4}$$

By applying the boundary condition to the above expression, we obtain

$$j(a^-) - j(a^+) = \frac{2\gamma}{\hbar}|\Psi(a)|^2 \tag{B.5}$$

$$j(-a^-) - j(-a^+) = -\frac{2\gamma}{\hbar}|\Psi(-a)|^2 \tag{B.6}$$

Therefore, the current flowing into the drain is proportial to the strength γ and also the density (or probability) of polariton at the boundary $|\Psi(a)|^2$. Similarly, for the boundary $x = -a$, the current flowing out of the darin is proportional to γ and $|\Psi(-a)|^2$.

Define the natrual length and energy units as

$$a_0 = \sqrt{\frac{\hbar}{2m\omega_0}} \quad \text{and} \quad \hbar\omega_0. \tag{B.7}$$

We have a harmonic potential problem in the bulk region. The stationary solution satisfies:

$$\frac{\partial^2}{\partial z^2}\Psi(z) + \left(\frac{E}{\hbar\omega_0} - \frac{1}{4}z^2\right)\Psi(z) = 0 \tag{B.8}$$

where we have changed variable $z = x/a_0$. This is of the standard form of Weber differential equation. One of it's linearly independent pair of solution is

$$D_\nu(z) \;\text{ and }\; D_\nu(-z), \quad \text{with } E = (\nu + 1/2)\hbar\omega_0 \tag{B.9}$$

where ν is a real and non-integer number.

Define the following trial wavefunction

$$\begin{cases} \Psi_{\mathrm{I}}(x) = CD_\nu(-z), & x < -\bar{a} \\ \Psi_{\mathrm{II}}(x) = AD_\nu(z) + BD_\nu(-z), & -\bar{a} < x < \bar{a} \\ \Psi_{\mathrm{III}}(x) = FD_\nu(z), & x > \bar{a} \end{cases} \tag{B.10}$$

where $\bar{a} = a/a_0$. Apply the above boundary conditions, we arrive at the secular equation for solving the coefficient A and B:

$$\begin{pmatrix} W(-\bar{a}) + 2i\bar{\gamma}D_\nu(\bar{a})D_\nu(-\bar{a}) & 2i\bar{\gamma}D_\nu(\bar{a})^2 \\ -2i\bar{\gamma}D_\nu(\bar{a})^2 & W(\bar{a}) - 2i\bar{\gamma}D_\nu(-\bar{a})D_\nu(\bar{a}) \end{pmatrix} \begin{pmatrix} A \\ B \end{pmatrix} = 0 \quad \text{(B.11)}$$

where $W_\nu(z)$ is the Wronskian of the two independent functions $D_\nu(z)$ and $D_\nu(-z)$ which is a constant given by $W(z) = (2\pi)^{1/2}/\Gamma(-\nu)$. $\bar{\gamma} = \gamma/(a \cdot \hbar\omega_0)$ is a dimensionless parameter. $\Gamma(-\nu)$ is the gamma function.

For the existence of nonzero solution, we must require the determinant of the matrix be 0, that is

$$\frac{2\pi}{\Gamma(-\nu)^2} = 4\bar{\gamma}^2 D_\nu(\bar{a})^2 \left(D_\nu(\bar{a})^2 - D_\nu(-\bar{a})^2\right) \quad \text{(B.12)}$$

where we note that $\Gamma(-\nu)$ approaches ∞ at integer ν. We found that there is a non-zero solution near each integer value of ν. We are interested in the solution near $\nu = 0$ which corresponds to the lowest energy bound state.

To compare the energy shift with experiment, we need to estimate $\hbar\omega_0$. We take the follwing approximate values from experiment: width of the potential trap $a \sim 5\mu m$, depth of the potential trap $V_0 \sim 1meV$ and effective mass of polaritons $m \sim 10^{-4} m_e$. Based on these parameters we find that

$$\hbar\omega_0 \approx 0.25meV \quad \text{and} \quad a_0 \approx 2\mu m \quad \text{(B.13)}$$

Therefore we see that $\bar{a} = a/a_0$ falls roughly in between $2 \sim 2.5$. We plot the energy using $E = (\nu + 1/2)\hbar\omega_0$ as shown in following Fig. B.3.

We also plot the normalized wavefunction and current distribution of the lowest bound state (see Fig. B.4).

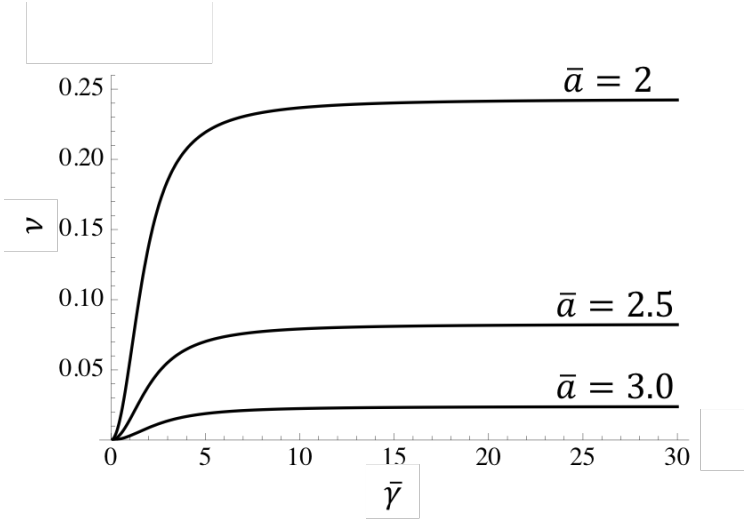

Figure B.2: Solution ν (related to energy by $E = (\nu + 1/2)\hbar\omega_0$) of the lowest bound state (ν near 0) as a function of strength $\bar{\gamma}$ for different value of the width a. The energy saturate at a finite value at large $\bar{\gamma}$. The saturation energy decreases as $\bar{a}$ increases.

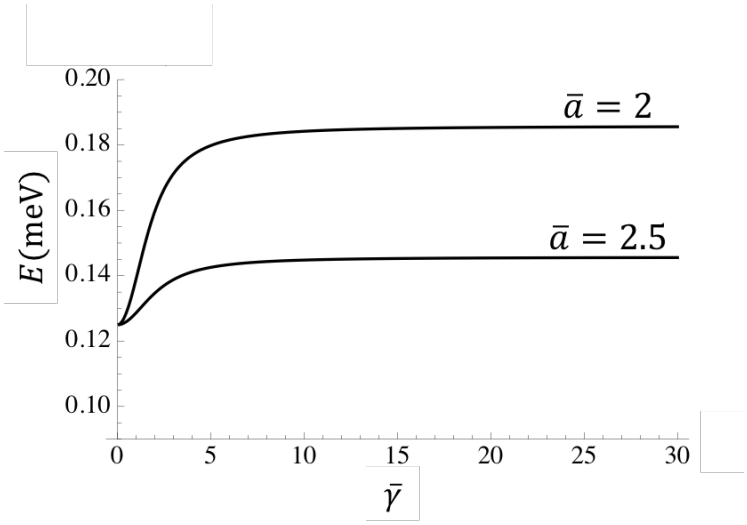

Figure B.3: Value of the energy estimate using approximate parameters given above. We have defined $\bar{\gamma} \equiv \gamma/(a_0 \cdot \hbar\omega_0)$.

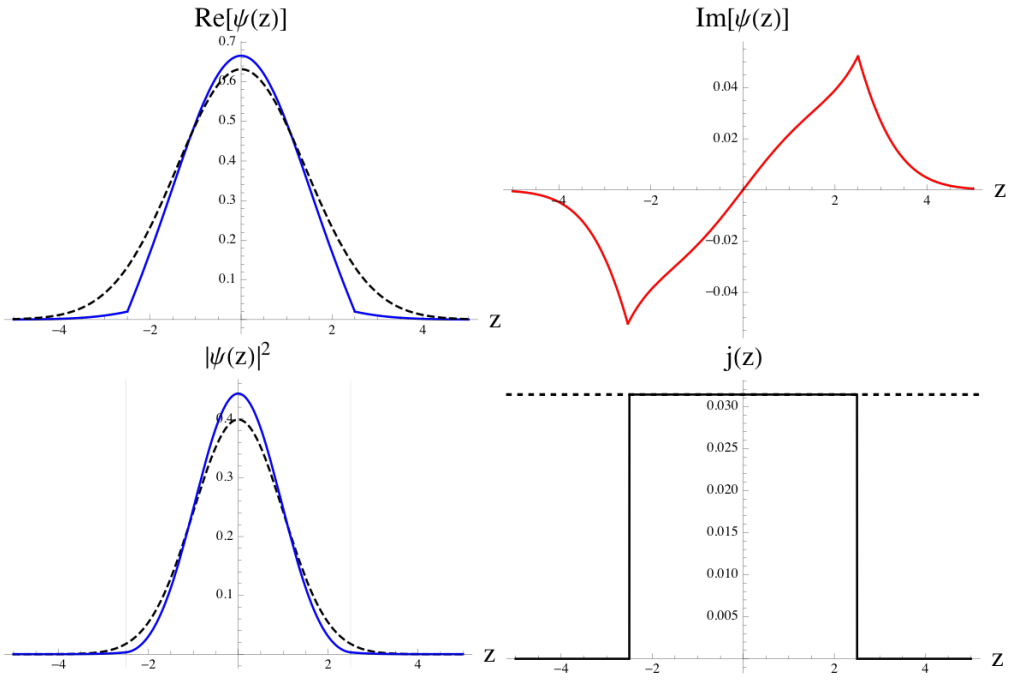

Figure B.4: Typical wavefunction and current distribution of the lowest bound state. Here we used $\bar{\gamma} = 5$ and $\bar{a} = 2.5$. The dashed curve in top-left and bottom-left graph represent the $n = 0$ state wavefunction of the usuall bare harmonic potential with no source and drain.

As we can see from the current distribution, it is finite only in the region between the source and the drain. The amplitude of the current for fixed density (normalized) is plotted below (Fig. B.5). It is obvious that the current is not a monotonic function of $\bar{\gamma}$ because it dependes on the product of $\bar{\gamma}$ and $|\Psi(-a)|^2$.

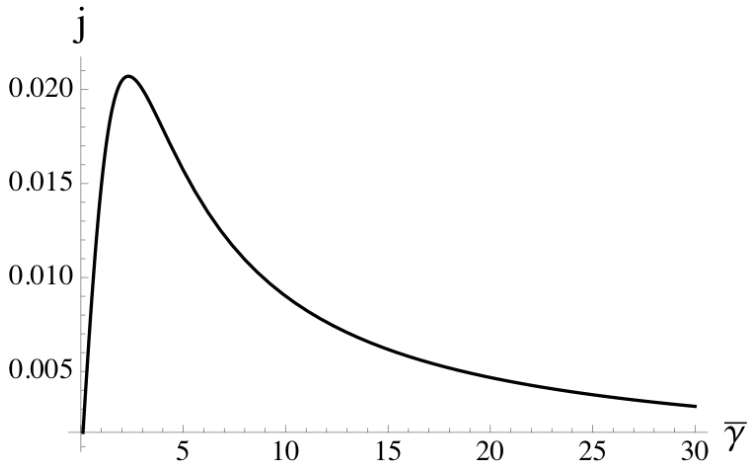

Figure B.5: Current in between the source and drain for fixed density of polaritons. We take $\bar{a} = 2.5$ here.

Publication List

1. **Ming Xie**, David Snoke, and Allan H. MacDonald, *Polariton supercurrent generation in unipolar electro-optic devices*, in preparetion arXiv: 1708.xxxx (2017)

2. **Ming Xie**, and Allan H. MacDonald, *Electrical reservoirs for spatially indirect two-dimensional excitons*, in preparetion arXiv: 1708.xxxx (2017)

3. **Ming Xie**, and Allan H. MacDonald, *Excitonic thermo-electric cooling device*, in preparetion (2017)

4. Fei Xue, Fengcheng Wu, **Ming Xie**, Jungjung Su, and Allan H. MacDonald, *Microscopic theory of equilibrium polariton condensates*, Phys. Rev. B, 94:235302, Dec 2016

5. **Ming Xie**, Guru Khalsa, and Allan H. MacDonald, *Optical conductivity of the t_{2g} two-dimensional electron gas*, Phys. Rev. B, 85:245417 (2014).

Bibliography

[1] M. H. Anderson, J. R. Ensher, M. R. Matthews, C. E. Wieman, and E. A. Cornell. Observation of Bose-Einstein condensation in a dilute atomic vapor. *Science*, 269(5221):198–201, 1995.

[2] L. Andreani, V. Savona, P. Schwendimann, and A. Quattropani. Polaritons in high reflectivity microcavities: semiclassical and full quantum treatment of optical properties. *Superlattices and Microstructures*, 15(4):453–458, 1994.

[3] F. Andreev. The thermal conductivity of the intermediate state in superconductors. *Sov Phys JETP*, pages 1228–1231, 11 1963.

[4] N. W. Ashcroft and N. D. Mermin. *Solid State Physics*. Brooks Cole, 1976.

[5] R. Balili, V. Hartwell, D. Snoke, L. Pfeiffer, and K. West. Bose-Einstein condensation of microcavity polaritons in a trap. *Science*, 316(5827):1007–1010, 2007.

[6] J. J. Baumberg, A. V. Kavokin, S. Christopoulos, A. J. D. Grundy, R. Butté, G. Christmann, D. D. Solnyshkov, G. Malpuech, G. Baldassarri Höger von Högersthal, E. Feltin, J.-F. Carlin, and N. Grandjean.

Spontaneous polarization buildup in a room-temperature polariton laser. *Phys. Rev. Lett.*, 101:136409, Sep 2008.

[7] P. W. Baumeister. Optical absorption of cuprous oxide. *Phys. Rev.*, 121:359–362, Jan 1961.

[8] P. Bhattacharya, T. Frost, S. Deshpande, M. Z. Baten, A. Hazari, and A. Das. Room temperature electrically injected polariton laser. *Phys. Rev. Lett.*, 112:236802, Jun 2014.

[9] P. Bhattacharya, B. Xiao, A. Das, S. Bhowmick, and J. Heo. Solid state electrically injected exciton-polariton laser. *Phys. Rev. Lett.*, 110:206403, May 2013.

[10] J. M. Blatt, K. W. Böer, and W. Brandt. Bose-Einstein condensation of excitons. *Phys. Rev.*, 126:1691–1692, Jun 1962.

[11] G. E. Blonder, M. Tinkham, and T. M. Klapwijk. Transition from metallic to tunneling regimes in superconducting microconstrictions: Excess current, charge imbalance, and supercurrent conversion. *Phys. Rev. B*, 25:4515–4532, Apr 1982.

[12] M. Born and K. Huang. *Dynamical Theory of Crystal Lattices*. Clarendon Press, 1954.

[13] A. Bramati and M. Modugno. *Physics of Quantum Fluids: New Trends and Hot Topics in Atomic and Polariton Condensates*. Springer, 2013.

[14] E. Burstein and S. Lundqvist. *Tunneling Phenomena in Solids*. Plenum Press, New York, 1969.

[15] E. Burstein and C. Weisbuch. *Confined Electrons and Photons: New Physics and Applications*. Springer, 1995.

[16] L. V. Butov, A. L. Ivanov, A. Imamoglu, P. B. Littlewood, A. A. Shashkin, V. T. Dolgopolov, K. L. Campman, and A. C. Gossard. Stimulated scattering of indirect excitons in coupled quantum wells: Signature of a degenerate Bose-gas of excitons. *Phys. Rev. Lett.*, 86:5608–5611, Jun 2001.

[17] L. V. Butov, C. W. Lai, A. L. Ivanov, A. C. Gossard, and D. S. Chemla. Towards bose-einstein condensation of excitons in potential traps. *Nature*, 417(6884):47–52, 05 2002.

[18] T. Byrnes, T. Horikiri, N. Ishida, and Y. Yamamoto. BCS wave-function approach to the BEC-BCS crossover of exciton-polariton condensates. *Phys. Rev. Lett.*, 105:186402, Oct 2010.

[19] T. Byrnes, N. Y. Kim, and Y. Yamamoto. Exciton-polariton condensates. *Nat Phys*, 10(11):803–813, 11 2014.

[20] I. Carusotto and C. Ciuti. Quantum fluids of light. *Rev. Mod. Phys.*, 85:299–366, Feb 2013.

[21] R. Casella. On the possibility of observing a Bose-Einstein condensation of excitons in CdS and CdSe. *Journal of Physics and Chemistry of Solids*, 24(1):19–26, 1963.

[22] C. Ciuti and I. Carusotto. Quantum fluid effects and parametric instabilities in microcavities. *physica status solidi (b)*, 242(11):2224–2245, 2005.

[23] M. Combescot, R. Combescot, and F. Dubin. Bose-Einstein condensation and indirect excitons: a review. *Reports on Progress in Physics*, 80(6):066501, 2017.

[24] Comte, C. and Nozires, P. Exciton Bose condensation : the ground state of an electron-hole gas - i. Mean field description of a simplified model. *J. Phys. France*, 43(7):1069–1081, 1982.

[25] P. Dawson, G. Duggan, H. I. Ralph, and K. Woodbridge. Free excitons in room-temperature photoluminescence of GaAs-$Al_xGa_{1-x}As$ multiple quantum wells. *Phys. Rev. B*, 28:7381–7383, Dec 1983.

[26] H. Deng, H. Haug, and Y. Yamamoto. Exciton-polariton Bose-Einstein condensation. *Rev. Mod. Phys.*, 82:1489–1537, May 2010.

[27] H. Deng, D. Press, S. Götzinger, G. S. Solomon, R. Hey, K. H. Ploog, and Y. Yamamoto. Quantum degenerate exciton-polaritons in thermal equilibrium. *Phys. Rev. Lett.*, 97:146402, Oct 2006.

[28] H. Deng, G. S. Solomon, R. Hey, K. H. Ploog, and Y. Yamamoto. Spatial coherence of a polariton condensate. *Phys. Rev. Lett.*, 99:126403, Sep 2007.

[29] H. Deng, G. Weihs, C. Santori, J. Bloch, and Y. Yamamoto. Condensation of semiconductor microcavity exciton polaritons. *Science*, 298(5591):199–202, 2002.

[30] F. J. DiSalvo. Thermoelectric cooling and power generation. *Science*, 285(5428):703–706, 1999.

[31] J. P. Eisenstein and A. H. MacDonald. Bose-Einstein condensation of excitons in bilayer electron systems. *Nature*, 432(7018):691–694, 12 2004.

[32] J. P. Eisenstein, L. N. Pfeiffer, and K. W. West. Independently contacted twodimensional electron systems in double quantum wells. *Applied Physics Letters*, 57(22):2324–2326, 1990.

[33] J. Frenkel. On the transformation of light into heat in solids. i. *Phys. Rev.*, 37:17–44, Jan 1931.

[34] J. Frenkel. On the transformation of light into heat in solids. ii. *Phys. Rev.*, 37:1276–1294, May 1931.

[35] A. K. Geim and I. V. Grigorieva. Van der Waals heterostructures. *Nature*, 499(7459):419–425, 07 2013.

[36] H. J. Goldsmid. *Introduction to Thermoelectricity*. Springer, 2010.

[37] A. V. Gorbunov and V. B. Timofeev. Collective state in a Bose gas of interacting interwell excitons. *JETP*, 83(4):146–151, 2006.

[38] A. A. High, J. R. Leonard, A. T. Hammack, M. M. Fogler, L. V. Butov, A. V. Kavokin, K. L. Campman, and A. C. Gossard. Spontaneous coherence in a cold exciton gas. *Nature*, 483(7391):584–588, 03 2012.

[39] A. A. High, J. R. Leonard, M. Remeika, L. V. Butov, M. Hanson, and A. C. Gossard. Condensation of excitons in a trap. *Nano Letters*, 12(5):2605–2609, 2012.

[40] J. N. Hodgson. *Optical Absorption and Dispersion in Solids*. Chapman and Hall LTD, 1970.

[41] J. J. Hopfield. Theory of the contribution of excitons to the complex dielectric constant of crystals. *Phys. Rev.*, 112:1555–1567, Dec 1958.

[42] R. Houdré, C. Weisbuch, R. P. Stanley, U. Oesterle, P. Pellandini, and M. Ilegems. Measurement of cavity-polariton dispersion curve from angle-resolved photoluminescence experiments. *Phys. Rev. Lett.*, 73:2043–2046, Oct 1994.

[43] K. Huang. On the interaction between the radiation field and ionic crystals. *Proceedings of the Royal Society of London A: Mathematical, Physical and Engineering Sciences*, 208(1094):352–365, 1951.

[44] A. Ioffe. *Semiconductor Thermoelements and Thermoelectric cooling*. Infosearch Limited London, 1957.

[45] A. F. Ioffe and L. S. Stil'bans. Physical problems of thermoelectricity. *Reports on Progress in Physics*, 22(1):167, 1959.

[46] D. Jérome, T. M. Rice, and W. Kohn. Excitonic insulator. *Phys. Rev.*, 158:462–475, Jun 1967.

[47] K. Kamide and T. Ogawa. What determines the wave function of electron-hole pairs in polariton condensates? *Phys. Rev. Lett.*, 105:056401, Jul 2010.

[48] J. Kasprzak, M. Richard, S. Kundermann, A. Baas, P. Jeambrun, J. M. J. Keeling, F. M. Marchetti, M. H. Szymanska, R. Andre, J. L. Staehli, V. Savona, P. B. Littlewood, B. Deveaud, and L. S. Dang. Bose-Einstein condensation of exciton polaritons. *Nature*, 443(7110):409–414, 09 2006.

[49] M. Kawabe, M. Kondo, N. Matsuura, and K. Yamamoto. Photoluminescence of Al_xGa_{1-x} As/Al_yGa_{1-y}As multiquantum wells grown by pulsed molecular beam epitaxy. *Japanese Journal of Applied Physics*, 22(2A):L64, 1983.

[50] L. V. Keldysh and A. N. Kozlov. Collective properties of excitons in semiconductors. *Sov. Phys. JETP*, 27:521, Sept. 1968.

[51] R. S. Knox. *Theory of Excitons*. Academic Press, 1963.

[52] S. W. Koch, M. Kira, G. Khitrova, and H. M. Gibbs. Semiconductor excitons in new light. *Nat Mater*, 5(7):523–531, 07 2006.

[53] T. Liew, I. Shelykh, and G. Malpuech. Polaritonic devices. *Physica E: Low-dimensional Systems and Nanostructures*, 43(9):1543–1568, 2011.

[54] Y. Lozovik and V. Yudson. Feasibility of superfluidity of paired spatially separated electrons and holes; a new superconductivity mechanism. *JETP Lett.*, 22:274, 1976.

[55] G. D. Mahan. Figure of merit for thermoelectrics. *Journal of Applied Physics*, 65(4):1578–1583, 1989.

[56] K. F. Mak, K. He, C. Lee, G. H. Lee, J. Hone, T. F. Heinz, and J. Shan. Tightly bound trions in monolayer MoS_2. *Nat Mater*, 12(3):207–211, 03 2013.

[57] K. F. Mak and J. Shan. Photonics and optoelectronics of 2D semiconductor transition metal dichalcogenides. *Nat Photon*, 10(4):216–226, 04 2016.

[58] S. A. Moskalenko and D. W. Snoke. *Bose-Einstein Condensation of Excitons and Biexcitons*. Cambridge University Press, 2000.

[59] D. A. Mylnikov, V. V. Belykh, N. N. Sibeldin, V. D. Kulakovskii, C. Schneider, S. Høfling, M. Kamp, and A. Forchel. Dynamics of spatial coherence and momentum distribution of polaritons in a semiconductor microcavity under conditions of Bose-Einstein condensation. *JETP Letters*, 101(8):513–518, Apr 2015.

[60] K. S. Novoselov, A. Mishchenko, A. Carvalho, and A. H. Castro Neto. 2D materials and Van der Waals heterostructures. *Science*, 353(6298):aac9439, 2016.

[61] M. Palummo, M. Bernardi, and J. C. Grossman. Exciton radiative lifetimes in two-dimensional transition metal dichalcogenides. *Nano Letters*, 15(5):2794–2800, 2015.

[62] S. Pekar. Theory of electromagnetic waves in a crystal with excitons. *Journal of Physics and Chemistry of Solids*, 5(1):11–22, 1958.

[63] G. Pitaevskii and S. Stringari. *Bose-Einstein Condensation*. Clarendon Press, 2003.

[64] D. Y. Qiu, F. H. da Jornada, and S. G. Louie. Optical spectrum of MoS_2: Many-body effects and diversity of exciton states. *Phys. Rev. Lett.*, 111:216805, Nov 2013.

[65] R. A. Riedel, L.-F. Chang, and P. F. Bagwell. Critical current and self-consistent order parameter of a superconductor–normal-metal–superconductor junction. *Phys. Rev. B*, 54:16082–16095, Dec 1996.

[66] P. Rivera, J. R. Schaibley, A. M. Jones, J. S. Ross, S. Wu, G. Aivazian, P. Klement, K. Seyler, G. Clark, N. J. Ghimire, J. Yan, D. G. Mandrus, W. Yao, and X. Xu. Observation of long-lived interlayer excitons in monolayer $MoSe_2$–WSe_2 heterostructures. *Nature Communications*, 6:6242, 02 2015.

[67] M. Rontani and L. J. Sham. Coherent transport in a homojunction between an excitonic insulator and semimetal. *Phys. Rev. Lett.*, 94:186404, May 2005.

[68] J. Sánchez-Cañizares and F. Sols. Self-consistent scattering description of transport in normal-superconductor structures. *Phys. Rev. B*, 55:531–543, Jan 1997.

[69] D. Sanvitto and S. Kena-Cohen. The road towards polaritonic devices. *Nat Mater*, 15(10):1061–1073, 10 2016.

[70] D. Sanvitto and V. Timofeev. *Exciton Polaritons in Microcavities*. Springer, 2012.

[71] D. Snoke. Spontaneous Bose coherence of excitons and polaritons. *Science*, 298(5597):1368–1372, 2002.

[72] D. Snoke and G. M. Kavoulakis. Bose-Einstein condensation of excitons in Cu_2O: progress over 30 years. *Reports on Progress in Physics*, 77(11):116501, 2014.

[73] J.-J. Su and A. H. MacDonald. How to make a bilayer exciton condensate flow. *Nat Phys*, 4(10):799–802, 10 2008.

[74] Y. Sun, P. Wen, Y. Yoon, G. Liu, M. Steger, L. N. Pfeiffer, K. West, D. W. Snoke, and K. A. Nelson. Bose-Einstein condensation of long-lifetime polaritons in thermal equilibrium. *Phys. Rev. Lett.*, 118:016602, Jan 2017.

[75] J. Snchez-Caizares and F. Sols. Transport in normal-superconductor-normal structures with local conservation of current. *Physica B: Condensed Matter*, 252(4):304–311, 1998.

[76] S. Takei and Y. Tserkovnyak. Superfluid spin transport through easy-plane ferromagnetic insulators. *Phys. Rev. Lett.*, 112:227201, Jun 2014.

[77] C. Uihlein, D. Fröhlich, and R. Kenklies. Investigation of exciton fine structure in Cu_2O. *Phys. Rev. B*, 23:2731–2740, Mar 1981.

[78] G. H. Wannier. The structure of electronic excitation levels in insulating crystals. *Phys. Rev.*, 52:191–197, Aug 1937.

[79] C. Weisbuch, M. Nishioka, A. Ishikawa, and Y. Arakawa. Observation of the coupled exciton-photon mode splitting in a semiconductor quantum microcavity. *Phys. Rev. Lett.*, 69:3314–3317, Dec 1992.

[80] E. Wertz, L. Ferrier, D. D. Solnyshkov, R. Johne, D. Sanvitto, A. Lemaitre, I. Sagnes, R. Grousson, A. V. Kavokin, P. Senellart, G. Malpuech, and J. Bloch. Spontaneous formation and optical manipulation of extended polariton condensates. *Nat Phys*, 6(11):860–864, 11 2010.

[81] R. Winkler. Excitons and fundamental absorption in quantum wells. *Phys. Rev. B*, 51:14395–14409, May 1995.

[82] F. Wooten. *Optical Properties of Solids*. Academic Press, 1972.

[83] F.-C. Wu, F. Xue, and A. H. MacDonald. Theory of two-dimensional spatially indirect equilibrium exciton condensates. *Phys. Rev. B*, 92:165121, Oct 2015.

[84] K. Wu, L. Rademaker, and J. Zaanen. Bilayer excitons in two-dimensional nanostructures for greatly enhanced thermoelectric efficiency. *Phys. Rev. Applied*, 2:054013, Nov 2014.

[85] J. Xia, F. Chen, J. Li, and N. Tao. Measurement of the quantum capacitance of graphene. *Nat. Nanotech.*, 4(8):505–509, 08 2009.

[86] M. Xie, G. Khalsa, and A. H. MacDonald. Optical conductivity of the t_{2g} two-dimensional electron gas. *Phys. Rev. B*, 89:245417, Jun 2014.

[87] F. Xue, F. Wu, M. Xie, J.-J. Su, and A. H. MacDonald. Microscopic theory of equilibrium polariton condensates. *Phys. Rev. B*, 94:235302, Dec 2016.

[88] I. Zapata and F. Sols. Andreev reflection in bosonic condensates. *Phys. Rev. Lett.*, 102:180405, May 2009.

[89] X. Zhu, P. B. Littlewood, M. S. Hybertsen, and T. M. Rice. Exciton condensate in semiconductor quantum well structures. *Phys. Rev. Lett.*, 74:1633–1636, Feb 1995.

Vita

Ming Xie was born in Shanshan, Xinjiang province, China in 1988. He received his Bachelor degree from Nanjing University in July 2010 in Nanjing, China. He started his graduate studies in the University of Texas at Austin in September 2010.

Permanent address: (e-mail) xiemphy@gmail.com

This dissertation was typeset with LaTeX[†] by the author.

[†]LaTeX is a document preparation system developed by Leslie Lamport as a special version of Donald Knuth's TeX Program.